CHARACTERIZATION OF MECHANICAL ADHESION FAILURE IN EPOXY

NANOCOMPOSITES BY ACOUSTIC EMISSION METHOD

A Thesis
Submitted to the Graduate Faculty
of the
North Dakota State University
of Agriculture and Applied Science

By

Matthew William Pearson

In Partial Fulfillment of the Requirements
for the Degree of
MASTER OF SCIENCE

Major Department:
Civil and Environmental Engineering

May 2021

Fargo, North Dakota

North Dakota State University
Graduate School

Title

CHARACTERIZATION OF MECHANICAL ADHESION FAILURE IN
EPOXY NANOCOMPOSITES BY ACOUSTIC EMISSION METHOD

By

Matthew William Pearson

The Supervisory Committee certifies that this **_disquisition_** complies with North Dakota State

University's regulations and meets the accepted standards for the degree of

MASTER OF SCIENCE

SUPERVISORY COMMITTEE:

Dr. Zhibin Lin

Chair

Dr. Mijia Yang

Dr. Long Jiang

Approved:

7/10/2021	Dr. Xuefeng Chu
Date	Department Chair

ABSTRACT

Polymeric nanocomposite coatings are used to protect metallic components in a variety of civil structures from corrosive agents. The adhesion between a coating and its substrate is not yet fully understood. In this study, the relationship between mechanical delamination of epoxy coating systems and the acoustic noise generated during failure was explored using acoustic emission. Three metrics were compared: a) mechanical loading data, b) post-test image processing, and c) acoustic emission data to gain insight into the coating-substrate layer. Neat epoxy and three epoxy nanocomposite systems modified with carbon nanotubes (CNTs), graphene (GNPs), and silica (SiO_2) were casted on mild steel at two different thicknesses via draw-down bar. Test results demonstrated that there was a correlation between mechanical adhesion/cohesion strength and resulting acoustic noise. The findings suggested that the higher thickness in the reinforced coatings provided for a greater cohesion failure area as well as higher volume of acoustic energy.

ACKNOWLEDGMENTS

TABLE OF CONTENTS

LIST OF TABLES

LIST OF FIGURES

LIST OF ABBREVIATIONS

NACE..National Association of Corrosion Engineers

GDP..Gross Domestic Product

NDT ....Non-destructive Testing

SHM..Structural Health Monitoring

AE ....Acoustic Emission

OGP..Oil & Gas Pipelines

FEM..Finite Element Method

PDE ....Photodefinable Epoxy

PWB..Printed Wiring Board

SEM ....Scanning Electron Microscopy

CNT..Carbon Nanotubes (Multi-Walled)

GNP..Graphene Nanoplatelets

CHAPTER 1. INTRODUCTION

1.1. Background

Modern civil transportation infrastructure depends on steel as its primary structural component due to its high strength, high toughness, and light weight. Two such civil transportation structures, bridges and oil and gas transmission pipelines, have relied extensively on structural steel since the 1930s when welding replaced rivets as a more efficient and effective method of connecting steel members[1], [2]. Ferrous in nature, exposed steel without protective alloys is susceptible to oxidation in aggressive environments and will eventually succumb to corrosion. Corrosion results in a reduction of cross-sectional area of steel members as well as surface damage that can lead to stress corrosion cracking and, if left untended, eventual structural failure.

According to an IMPACT study conducted by NACE, the global annual cost of corrosion repair, maintenance, and failure is estimated to be $2.5 trillion USD which equals approximately 3.4% of the global GDP[3]. The United States faces a significant volume of domestic corrosion related failures every year. PHMSA's database shows that in the United States pipeline industry, corrosion has accounted for 17% of all pipeline failures between 2009-2018[4]. Additionally, in 2013, NACE reported that the annual direct cost of corrosion in highway bridges in the United States was estimated at $13.6 billion USD[5]. Serious attention and care have been paid to corrosion protection, monitoring, and repair in order to mitigate these costs and reduce threat of future catastrophic structural failure.

Epoxy coatings have been an attractive solution for corrosion protection since the 1970s in both oil and gas transmission lines as well as bridge deck reinforcement[6], [7]. Ideal mechanical properties, reliable chemical resistance, and strong adhesion are some of the driving factors that make epoxy such a widely used thermoset polymer across many industries[8]. Although epoxy already has many ideal properties for numerous applications, the incorporation of nanofillers into epoxy

composites in recent decades has given way to significant enhancements in its performance and expanded its utility[9], [10].

1.2. Problem Statement

In structures where the coating is not visible or easily testable, such as bridge reinforcement and the interior/exterior surface of underground pipelines, damage detection and monitoring of corrosion due to coating delamination can be difficult. Non-Destructive Testing methods are essential in Structural Health Monitoring of civil transportation structures to avoid shutdown costs during their service life. Acoustic emission has seen extensive use in the SHM of bridges and oil and gas pipelines due to its high sensitivity to detect possible sources of displacement, stress, and strain across long distances.

Epoxy nanocomposites are becoming more widely used as a protective coating system in modern civil structures containing metallic structural elements subjected to aggressive environmental elements. The polymer's adhesion to its substrate is an integral part of where the coating's protective strength comes from. As corrosive agents penetrate through the coating to the substrate, they will delaminate the coating and expose the steel beneath, making it vulnerable to corrosion.

There has been extensive research involving AE that aims to characterize the bulk mechanical properties of epoxy composites and nanocomposites. Although the research gives valuable information on the material properties of the epoxy composite material, it rarely explores in depth the mechanical adherence of epoxy coatings to its substrate. Identifying and characterizing coating delamination before corrosion progresses could help mitigate the immense cost and damage to property and the environment and the loss of life due to corrosion failures in our societal transportation infrastructure.

1.3. Research Objectives

The goal of this research is to use acoustic emission sensors to investigate mechanical adhesion between steel and epoxy-based coatings enhanced with different nanoparticles. The main objectives of this study are as follows:

1. Investigate the relationship between acoustic signals and adhesion strength.

2. Identify different failure modes and relate them to the captured acoustic signals in an effort to enhance the results of existing testing standards.

3. Compare and contrast signals obtained between epoxy coating systems with 3 different nanoparticle additives and 2 differing thicknesses.

1.4. Thesis Organization

This document is organized into 6 separate chapters as follows: Chapters 1 and 2 introduce protective coatings for corrosion protection and using acoustic emission as an NDT method. Chapter 2 also reviews and reflects on recent existing studies on mechanical adhesion of epoxy coatings. Fundamental concepts of coating adhesion and acoustic emission are laid out in Chapter 3 and the experimental setup is outlined in Chapter 4. Experimental results and analysis are displayed in Chapter 5. The final summary of the document, conclusions of the results, and future proceedings are presented in Chapter 6.

CHAPTER 2. LITERATURE REVIEW

2.1. Introduction

Modern steel structures designed for civil purposes typically require coatings as a means of protection from their environment. OGP are at the backbone of modern society's energy needs and require internal and external coatings for corrosion protection. In a report submitted to PHMSA in 2008, it was found that corrosion played a role in 23.6% of all hazardous liquid pipeline failures as well as 23.3% of all gas transmission line failures from 1988-2008 in the United States. PHMSA further reported that corrosion was responsible for 17% of failures in all United States pipelines from 2009-2018[4]. Additionally, Canada reported that 50% of all their pipeline failures from 2000-2006 were heavily impacted by corrosion[7]. These failures accumulated billions of USD in cost to citizens, the government, and oil companies as well as irreparable damage to the environment[7], [11]–[13]. Although many reported pipeline failures are small leaks[12], some can have catastrophic results. An explosion from a crude oil pipeline in Qingdao, China killed 62 and injured another 136 in 2013 where the main contributing failure mechanism was accelerated corrosion that was not caught during inspections[14]. The global consumption of oil per day in 2012 was 90 million barrels per day and is projected to hit 121 million per day by 2040, an increase of 34%[13]. As society prepares to move to renewable energy, it is important to take care when supplying chemical and mechanical protection to new pipelines to ensure minimal loss of economic cost, property damage, and life as the demand for oil and natural gas increases in the future.

Adhesion of polymers has been studied extensively, but still causes clashes of opinion in the scientific and academic community. There are 2 general primary mechanisms (both also containing several smaller contributory mechanisms) that influence a coating's adherence to its substrate: chemical adhesion and adsorption and mechanical interlocking[15], [16]. Although the phenomena have been thoroughly explored, it is still disagreed upon if a polymer's chemical resistance to corrosive

agents depends on its mechanical adherence to its substrate. Myshkin et al. has done extensive research in the field of polymer tribology and adhesion in recent decades. They have done broad studies on the factors that influence polymer adhesion without attributing adhesive strength exclusively to a single factor[16]–[20]. There is a general consensus that an all-encompassing theory is the end goal in explaining adhesion in polymers[21]–[25]. It is clear from the existing research in polymer adhesion that even more investigation and characterization of adhesion in polymer coatings is needed to fully understand their nature in order to more effectively engineer them for everyday uses.

2.2. Adhesive Strength in Structural Coatings

2.2.1. Adhesion of Structural Steel Coatings

High mechanical adhesion strength in coatings is desirable in civil structures to provide stronger resistance to external forces during installation and internal stresses during service life of the member. Thermosetting powder coatings such as fusion-bonded epoxy (FBE) has been historically used for the protection of structural steel components since the 1960s in pipelines and the 1970s for bridge deck reinforcement [26], [27]. FBE's adhesion to metallic components in structures is an essential element of their field performance.

Chang et al. [28] investigated recent reports (around 2008) of delamination at the steel interface of 3LPE (FBE with a polyethylene topcoat) pipeline coatings. Although the initial pull-off results indicated exceptionally high adhesion strength of 8,000 psi (55 MPa), water ingress into the epoxy (Fig. 2.1) and residual stresses from the high modulus and thermal expansion coefficient were both attributed in the delamination phenomenon observed. Inadequate formulation and application of the coating were recommended as procedures to improve to avoid future delamination.
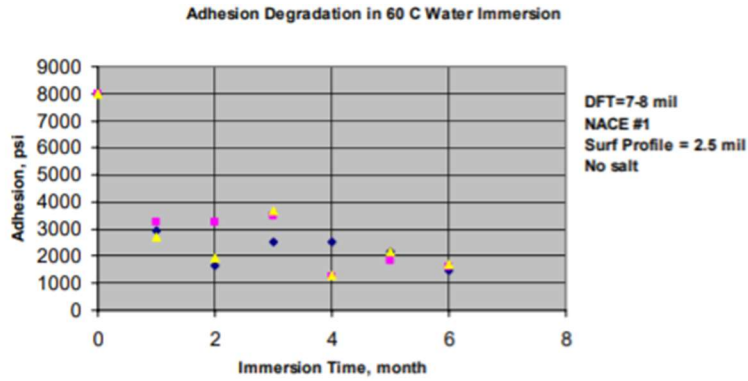
Figure 2.1: Adhesion Degradation for FBE in 60 °C water immersion [28]

Legghe et al. [29] observed a similar phenomenon by comparing water diffusion through epoxy to time of adhesion loss. The results reported were correlative for coating thickness below 250 μm but did not hold beyond that thickness as seen in Fig. 2.2 (500 μm was the max thickness tested). The author remarked that another phenomenon must be taking place within the coating structure, most likely resulting from changes in internal stress in the coating, leading to a more rapid interfacial disbondment.
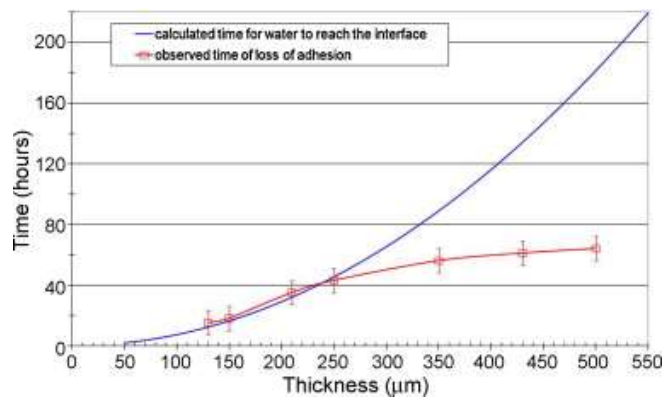
Figure 2.2: Saturation time and time of loss of adhesion vs. thickness [29]

It is clear from the present literature that there is a lack of understanding of the delamination mechanisms involved in this commonly used structural coating. Although water ingress to the substrate is responsible for part of the delamination phenomenon, there is another factor that is not

easily explained. A comprehensive characterization of the mechanical delamination phenomenon in epoxy coatings would give insight into this issue.

2.2.2. Adhesion of Epoxy-Based Nanocomposites

Thermoset liquid polymer coatings have gained popularity for pipeline and bridge component coatings due to their corrosion protection, low impact to the environment (due to low solvent content), and economic efficiency[6], [30]. Epoxy resins are very popular in industry due to their superior advantages in mechanical properties, strong adhesion, low shrinkage, and high chemical resistance, among others[8]. Although epoxy is a high performing thermoset polymer, a major disadvantage of epoxy is its characteristic surface defects present after curing that are natural pathways for water, oxygen, and corrosive ions to permeate through to the substrate. Undesirable pathways to the substrate severely hinder epoxy's long-term protection capabilities. This disadvantage has given way to research on additives such as nanoparticles that enhance epoxy's already strong properties while also helping to diminish its major surface defect flaw[31]. Epoxy nanocomposites have already been used in structural paints and coatings in civil infrastructure, with further applications being researched and developed[10]. This review focuses on recent literature exploring adhesion of epoxy nanocomposites.

Carbon nanotubes have high surface area, conductivity, and flexibility making them an ideal additive in epoxy composite coating systems[8]. Jeon et al. [32] observed an increase of adhesive strength when multi-walled carbon nanotubes were added into an epoxy coating. The increase in adhesive strength maintained following a hygrothermal cyclic test where the coating is subjected to heat and moisture repeatedly, highlighting its benefit further as seen in Fig. 2.3. The results also exhibited lower levels of water diffusion in the samples containing carbon nanotubes. Hedia et al. [33] explored the cohesive strength of epoxy enhanced with carbon nanotubes. SEM imaging (Fig. 2.4)

shows a fracture surface indicating that the high surface contact between the epoxy resin and nanotubes correlates to higher absorption of fracture energy at the molecular level as the force distribution is required to travel around the nanoparticles at the microscale.
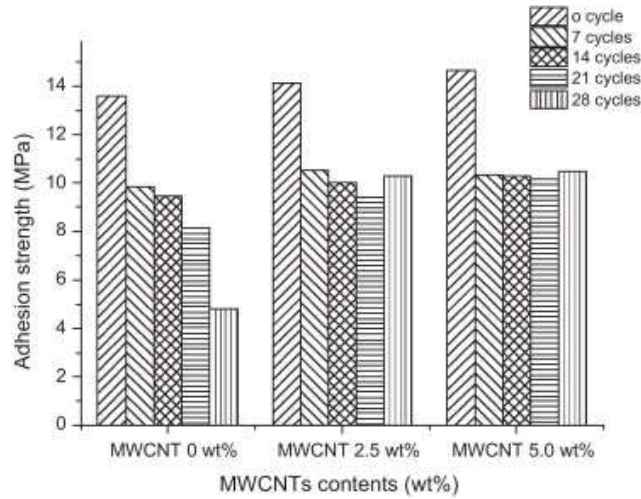
Figure 2.3: Pull-off adhesion strength of epoxy-coated carbon steel in terms of MWCNTs content with hygrothermal cyclic test [32]

| a | b |
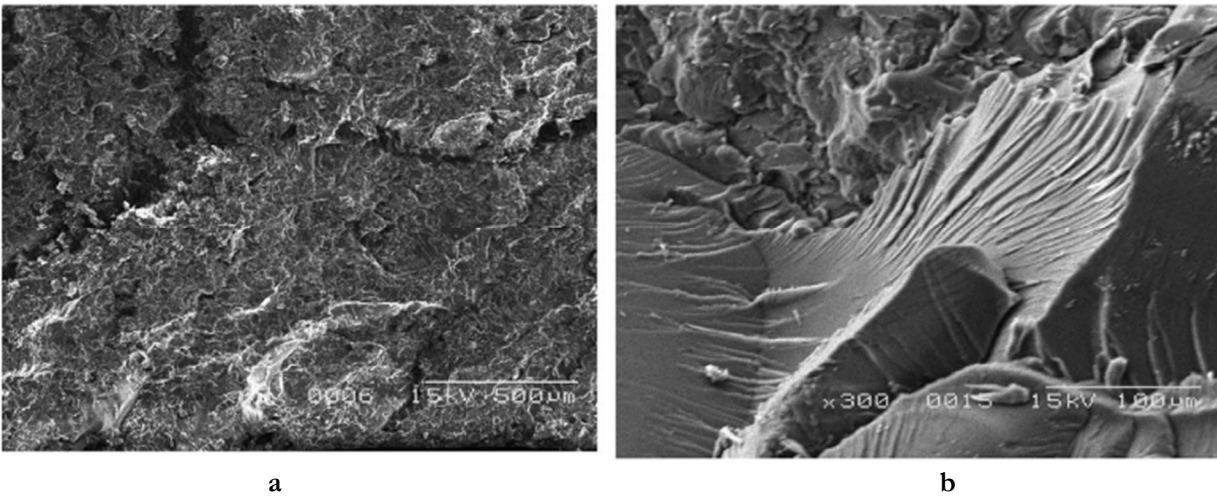
Figure 2.4: Scanning electron micrographs of the fracture surfaces of a neat epoxy 828-notched specimen (a) and MWCNT notched specimen (b).[33]

Another carbon-based nanomaterial, graphene, has seen popularity in recent decades as an additive for epoxy nanocomposites due to its incredible barrier and mechanical properties[34]–[36].

Alhumade et al. [37] explored adhesion in epoxy/graphene composites on stainless steel. The adhesion test results (using ASTM D3359 adhesion tape test) showed no delamination in 0.1% and 0.5% filler content before and after 60 days submerged in 3.5% NaCl solution as seen in Fig. 2.5. They further reported that as the filler content is increased past its critical point, a significant interfacial gap between coating and substrate was observed due to agglomerations which compromised adhesive strength as seen in Fig. 2.6. Monetta et al. [38] investigated graphene/epoxy composites on aluminum substrates and found little impact on chemical adhesion after graphene was added, remarking that the adhesion was considered "sufficient" without quantitative data reported. Wang et al. [39] found that graphene did not significantly increase the mechanical adhesion strength when incorporated into the epoxy matrix. Quantitative testing data on the topic of interfacial substrate mechanical adhesion in epoxy/graphene nanocomposites is not readily available.
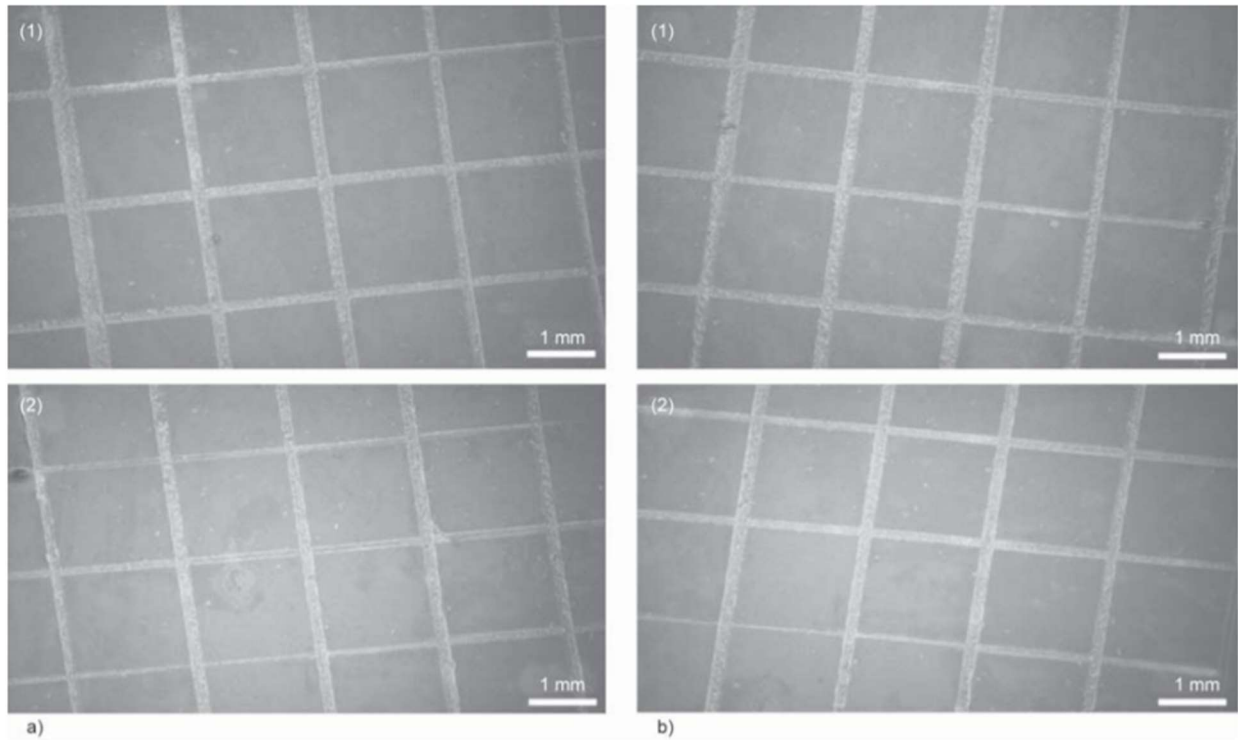
Figure 2.5: SEM images of post-adhesion tests of (1) E/G0.1 and (2) E/G0.5 coated SS304 substrates (a) before and (b) after 60 days of exposure to the corrosive medium [37]
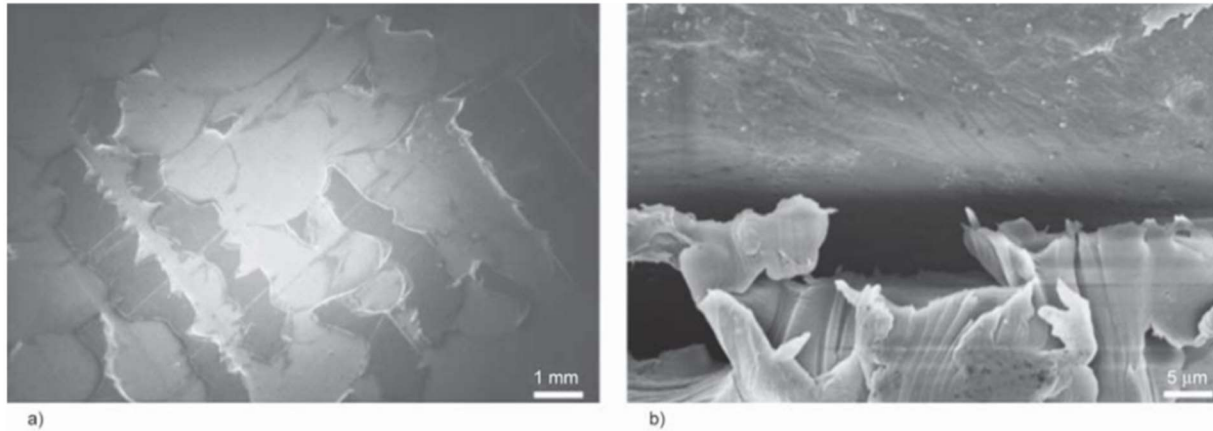
Figure 2.6: SEM image of (a) post-adhesion test and (b) cross section view of E/G1 coated SS304 substrate [37]

Nanosilica (SiO_2) has been used extensively in recent epoxy coating systems due to its superior barrier properties and its favorable chemical reactions with metal substrates and other nanofillers[40]–[44]. Pourhashem et al. [43] incorporated graphene-oxide/nanosilica hybrid (via a silane coupling agent) into an epoxy matrix. They saw a dramatic increase in adhesion strength due to silica-oxygen bonds at the coating-metal interface of nearly 100%. The failure mode observed during ASTM D4541 shifted from adhesive to cohesive when nanosilica was introduced (Fig. 2.7 and 2.8). Han et al. [45] reported on an increase of fracture toughness when nanosilica was added to an epoxy matrix. Fig. 2.9 shows a clear positive trend when the nanosilica is incorporated, even after 30 days of salt water immersion. Epoxy integrated with nanosilica has gained notoriety for its strong barrier properties and even higher performance with the addition of other nanomaterials. The mechanical adhesive strength and epoxy with unmodified nanosilica is seldom reported in literature.
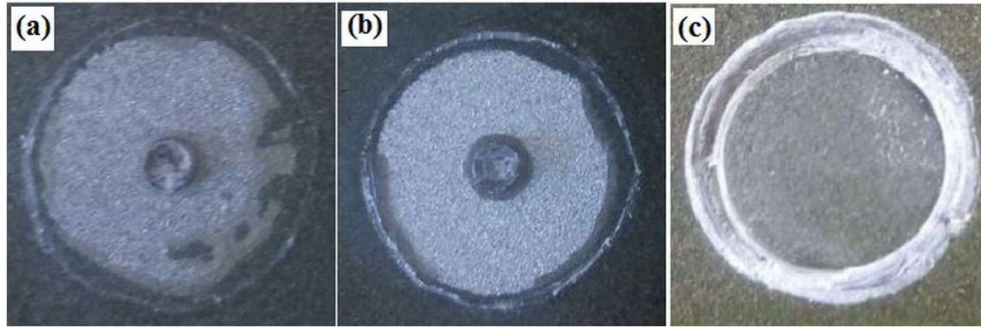
Figure 2.7: Visual performance of (a) pure epoxy, (b) epoxy/GO, and (c) epoxy/SiO₂-GO samples after pull-off adhesion test [43]
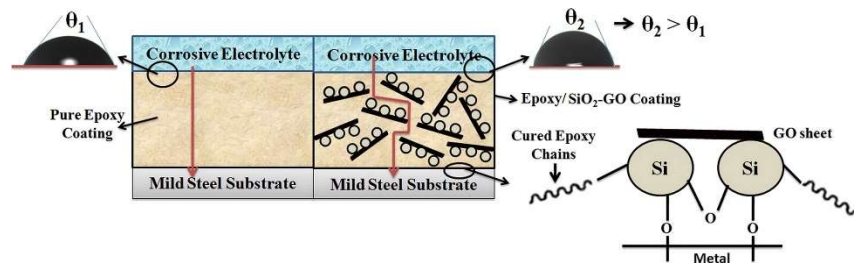
Figure 2.8: The schematic of corrosion protection mechanism for epoxy/SiO₂-GO nanocomposite coatings [43]
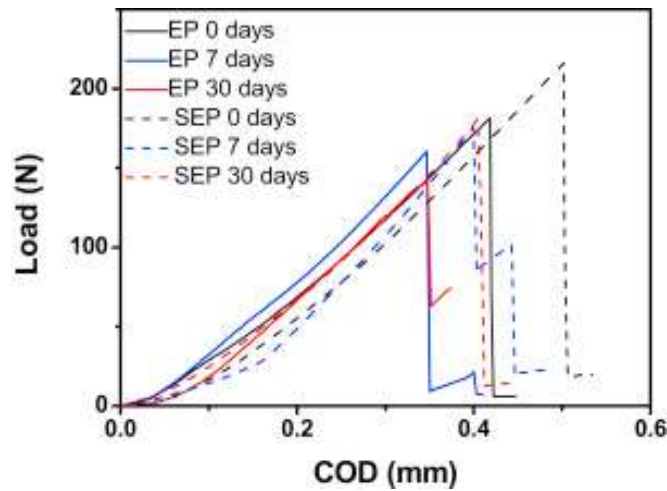
Figure 2.9: Typical load-crack opening displacement (COD) curves for neat epoxy (EP) and nanosilica enhanced epoxy composite (SEP) with different periods of immersion of 0, 7 and 30 days[45]

It is noted that differences in materials, dispersion, sample preparation, and test methodology are all impactful on the results obtained between each publication reviewed. Characterizing and comparing mechanical adhesion and cohesion mechanisms between different epoxy nanocomposite systems can provide insight into the fundamental theories of substrate adhesion and fracture mechanisms of polymer coatings as well as their individual performance in service. As nanomaterials are incorporated into epoxy-composite systems for modern day applications, analyzing adhesion test results between different coating systems is valuable information in characterizing them.

2.2.3. Detection of Adhesive Failure in Organic Coatings by Acoustic Emission

Acoustic emission sensors have been used since the 1960s as an effective means for passive SHM of bridges and OGP[46]–[48]. During fabrication and installation, structural members with thermoset polymer coatings are prone to natural and man-made defects (pinholes or holidays). These defects in most cases are unavoidable due to the nature of coating application and curing process. These defects can make substrates more accessible to corrosive agents that initiate and promote localized delamination, blistering, and corrosion on protected metallic surfaces. Detecting the delamination before it progresses is essential in SHM during the service lifespan of the structure. Acoustic emission was first used to capture coating adhesion failures while conducting the adhesion scratch test in a lab setting[49]. Articles are reviewed on existing studies of delamination and corrosion monitoring in organic coatings by acoustic emission methods.

Conradi et al. [50] used acoustic emission to monitor coating damage in a 3-point bending test of a epoxy/silica nanocomposite on steel (Fig. 2.10). The silica significantly increased the damage resistance of the coating compared to the neat epoxy. The signals produced during testing were divided into three frequency ranges of 90-200 kHz, 500-800 kHz, and 1200 kHz; each frequency range corresponding to matrix cracking during low strain, micro-debonding of the silica particles during

medium strain, and delamination of the coating away from the steel substrate at high strain, respectively (Fig 2.11). The abundance of signals present in the data from the silica samples helped to characterize the failure mechanisms experienced during loading more effectively than the neat epoxy sample.
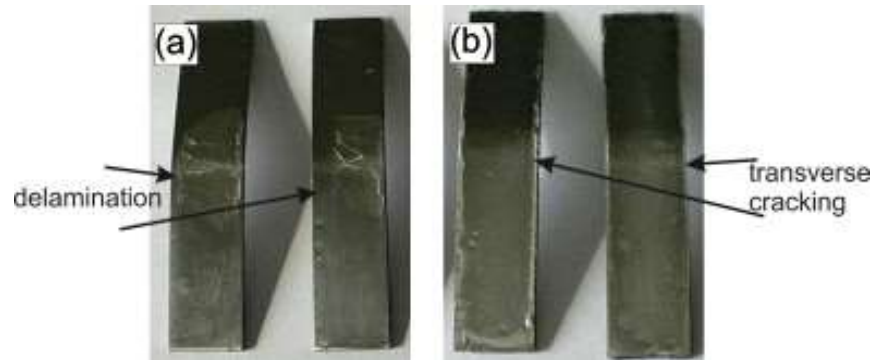
Figure 2.10: Photo images of the damaged samples after completed 3PB test: (a) two samples of DSS 2205 covered with epoxy coating and (b) two samples of DSS 2205 covered with 130-nm silica/epoxy coating [50]
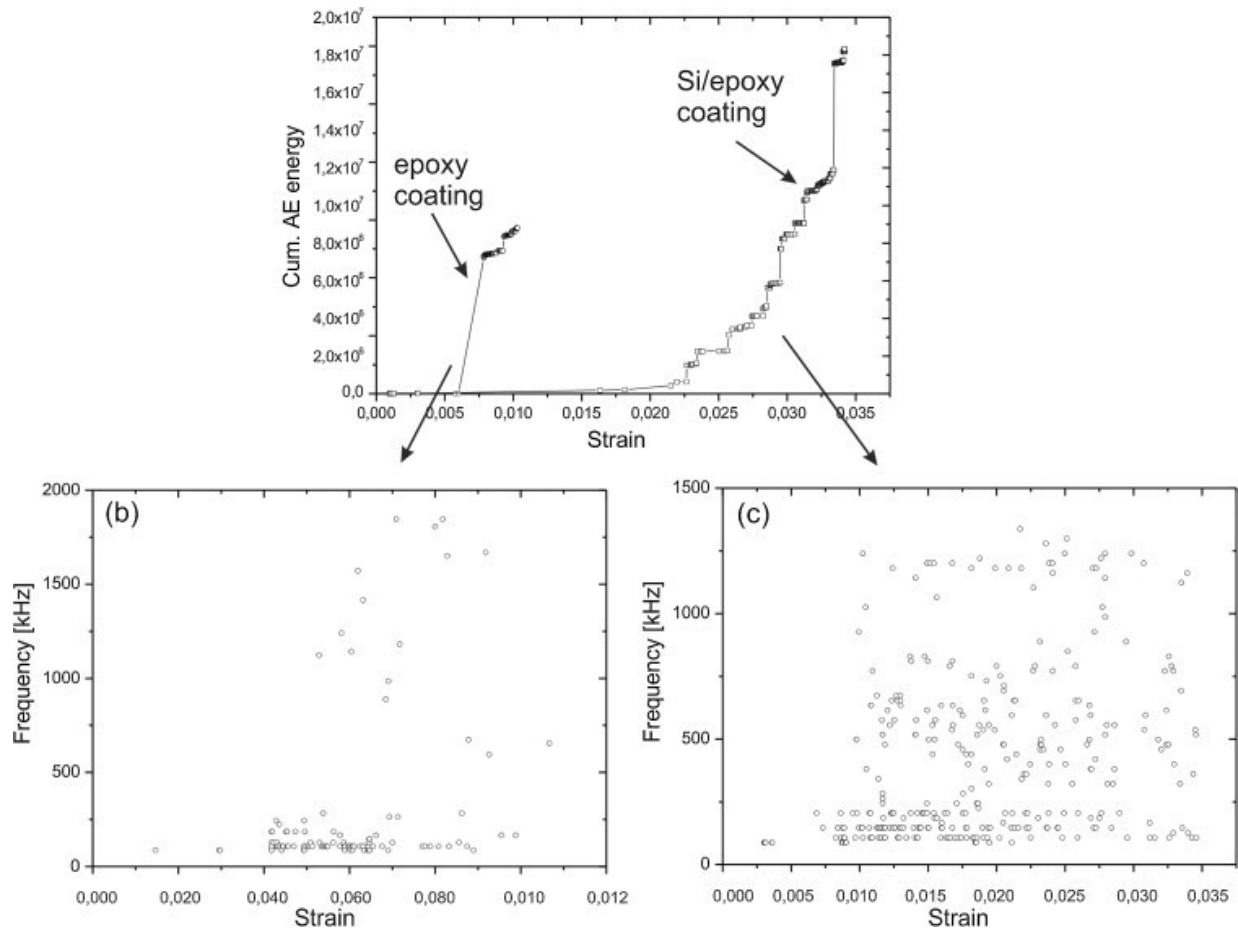
Figure 2.11: Acoustic emission diagrams (a) and frequency content of acoustic emission for 3PB test on DSS 2205 plate coated with epoxy (b) and 130-nm silica/epoxy (c) coatings [50]

Baltiz et al. [51] explored the feasibility of using acoustic emission to monitor corrosion on an aluminum substrate coated with epoxy modified with carbon nanotubes and graphite. The samples were polarized to induce corrosion by running a cycle of cathodic and anodic currents through them. Neat epoxy samples were found to have a very high volume of signals in the beginning of the tests, hypothesized that the water intake of the samples caused matrix cracking which produced the signals. The signals seen in the samples containing carbon nanotubes did not exhibit the same phenomenon, but a more gradual step-like noise progression. The author proceeded to speculate that the nanoparticles may have filled in the voids present in the epoxy, forcing the water to weave between the particles during swelling, causing slower water ingress and noise generation. In this study, it was

reported that acoustic emission could have effectively detected the formation of hydrogen bubbles, epoxy degradation (swelling and micro cracking), and interfacial degradation and water transport at the nonfiller/epoxy interface. The graphical representations of the EIS/acoustic data is displayed in Fig. 2.12 (a, b, c). It is stated that more studies are required to characterize acoustic emission signals received from corrosion events to verify the integrity of the results.
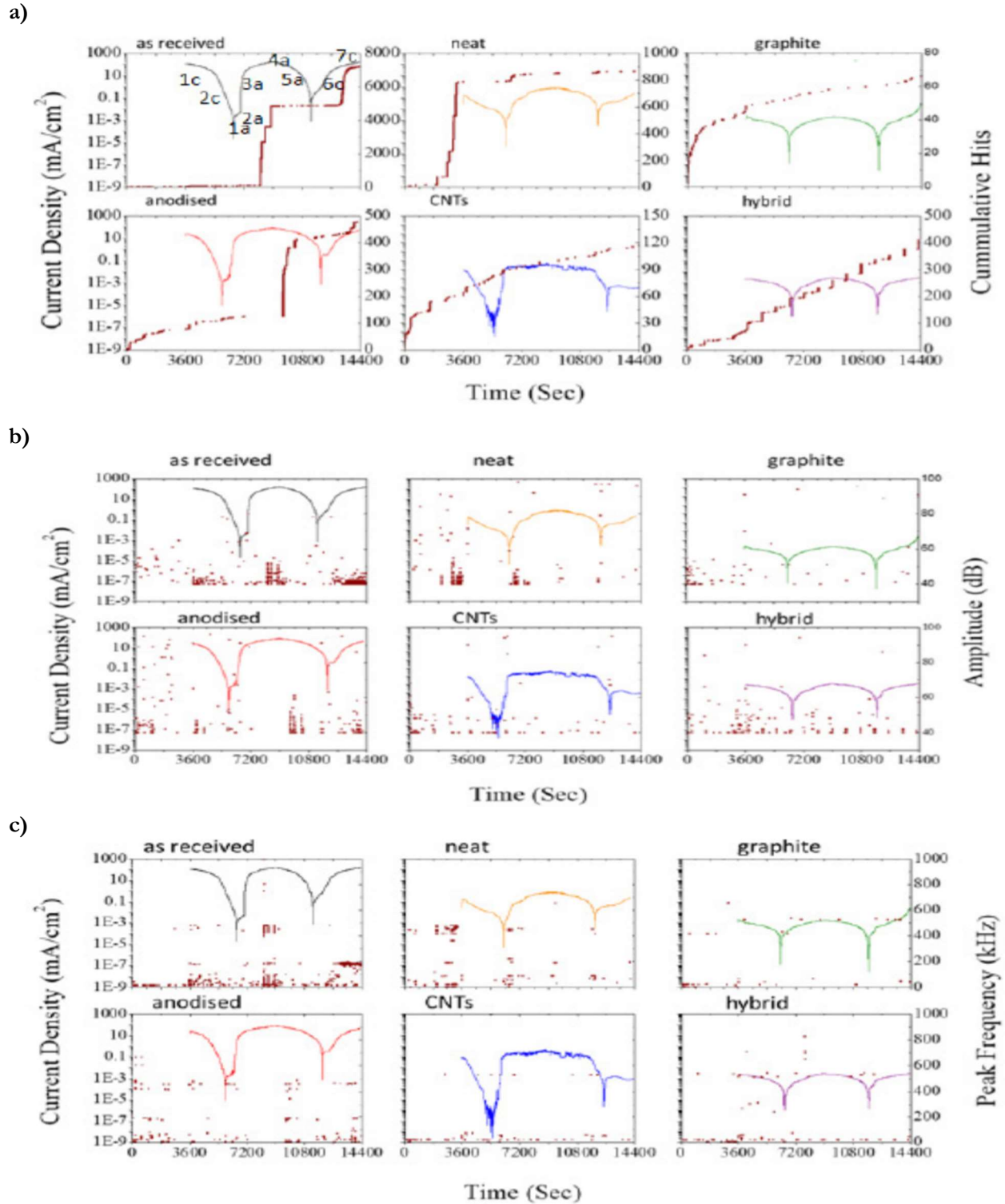
Figure 2.12: Current density and cumulative AE hit (a), amplitude (b), and peak frequency (c) vs. time curves for all tested specimens un-coated and coated [51]

16

2.2.4. Testing Standard for Mechanical Adhesion of Organic Coatings

ASTM D4541 provides a testing standard for measuring coating adhesion and is widely used to characterize adhesion of many coating materials in various industries. Simply put, the test involves gluing an aluminum dolly to a material's surface and then being ripped off using one of several different approved testing machines. The results are reported in psi for the final loading pressure measured before adhesive failure. The tested delaminated area is also reported as percent values denoted by either adhesive or cohesive failure. Fig. 2.13 shows a schematic of the testing method [52]. Although the test is widely used, there are issues with the test's precision, practicality, and simplistic result reporting that leaves some lab tests with incomplete or even inaccurate representations of the coating's mechanical adherence, not to mention the issues posed with in situ testing of existing structures[52]–[58]. Schilling [53] remarks on the variation present in acceptable results obtained from the ASTM D4541 test, stating that the "acceptable percent-age difference between two values may be between about 25% and 58%.". This variability in the testing method can cause concern when results can have such a vast range, making the method lack precision and repeatability in some scenarios.
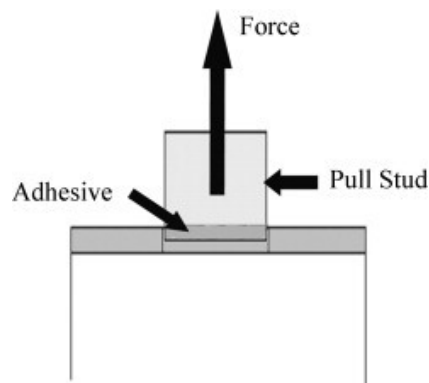
Figure 2.13: Fundamental pull-off adhesion test [23]

Ramos et al. [55] conducted a statistical reliability study across 55 case studies using a similar pull-off method used for the in situ measuring of the adhesive strength of cement-based adhesives and renderings designed to adhere ceramic tiles to building façade. The results showed large standard

deviations for the in-situ tests (Fig. 2.14) compared to the lab tests (Fig. 2.15). The study concludes by stating that even though there was an abundance of statistical data to be analyzed, there was still not sufficient evidence for correlative conclusions and without modifications to future pull-off testing on the materials in question, the results collected were prone to significant data variation. Flores-Colen et al. [59] reported similar findings in the 8 case studies investigated in that study, shown in Fig. 2.16. The unreliability and semi-destructive nature of the pull-off method analyzed lead the author to suggest other testing methods such as ultrasonic assessment for the inspection of ceramic building façade tiles.

a)
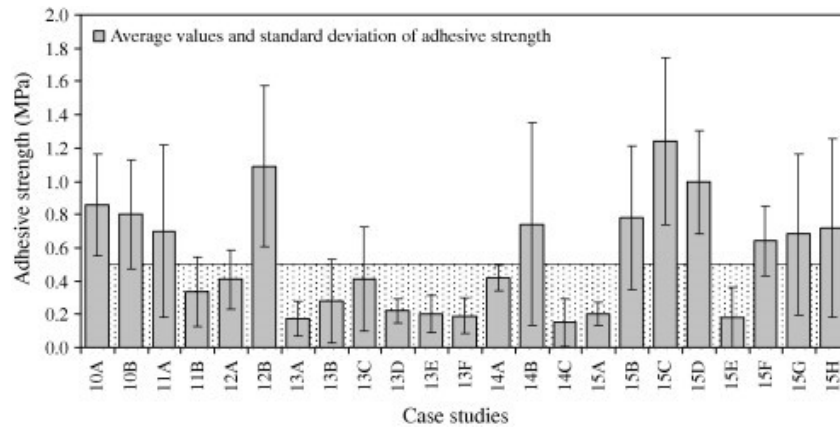
b)
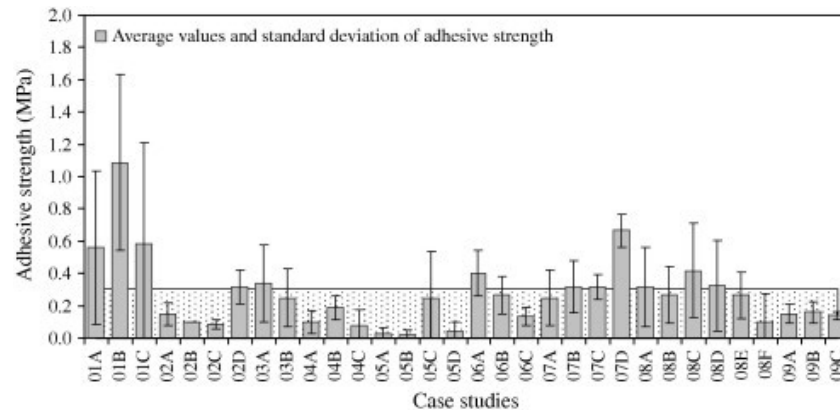
Figure 2.14: Average values and standard deviation of adhesive strength for cement based adhesives (a) and rendering (b) case studies [55]

18
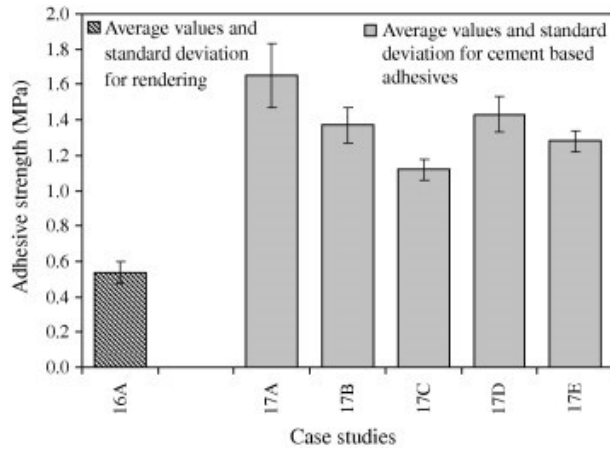
Figure 2.15: Average values and standard deviation for laboratory tests [55]
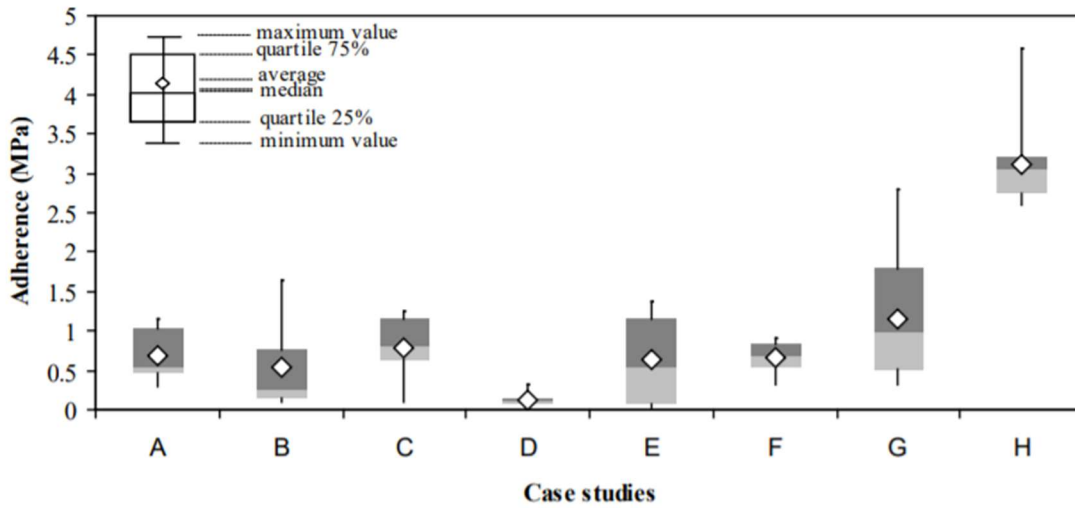
Figure 2.16: Box-plot diagram with the pull-off test results for the eight case studies [59]

Turunen et al. [56] conducted FEM to analyze the effect a flexible substrate had on the epoxy adhesive used to secure the dollies in pull-off testing of a photodefinable epoxy coating from a copper wiring board substrate. It was found that a dramatic increase in stress was found at the edge of the dollies and severely reduced the adhesive capacity in the sample. In their efforts to investigate the PDE/PWB interface, the bending in the PDE substrate (without proper sample preparation) tended to shift the failure to the adhesive/PDE interface. The measured stress capacity at the PDE/copper interface was 50% higher when using their "rigid" test setup as opposed to their "flexible" setup. Fig

19

2.17 shows the FEM results in detail. The pull-off test provides a starting point for mechanical adhesion evaluation of a coating on a substrate, but lacks the depth needed in certain tests such as the aforementioned.
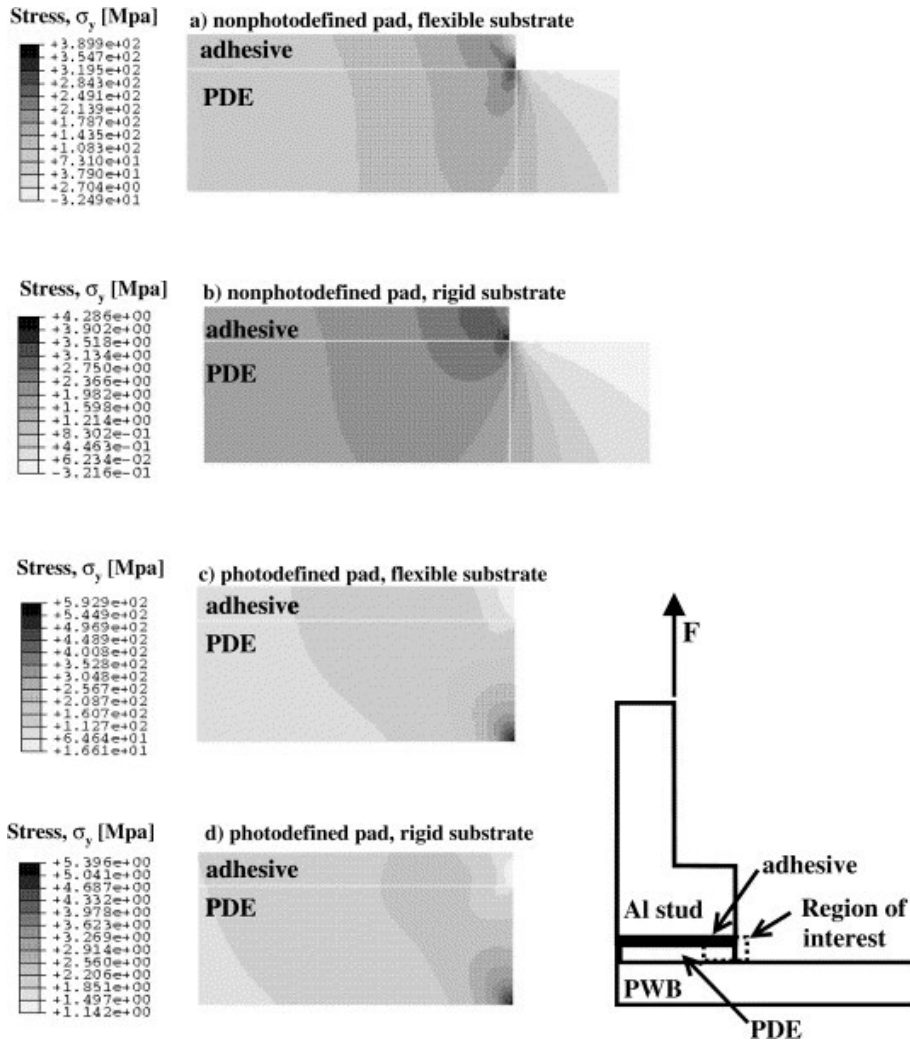
Figure 2.17: Calculated tensile stress distributions in the vicinity of the stud edge: (a) the nonphotodefined test pad on flexible substrate, (b) nonphotodefined test pad on rigid substrate, (c) photodefined test pad on flexible substrate, and (d) photodefined test pad on rigid substrate [56]

A thoughtful approach is required for more complicated sample testing and some tests require modified pull-off tests to accommodate. Croll et al. [57] investigated the reliability of the pull-off test on a polyurethane coating for steel water pipelines. Pipelines come with undesirable geometry for the traditional pull-off test, requiring a lot of sample preparation to make acceptable alignments for when

20

the dolly is pulled off. Reported issues inherent to the curved surface in relation to the dollies included air bubbles, dolly sliding, glue retraction, and scoring issues, among others. In over 1000 individual adhesion tests with multiple variables controlled and optimized in this study, Croll et al. a standard deviation as high as 20%. It is stated by the authors that "employing pull-off adhesion as the primary factor in gauging coating service life is not justified due to the intrinsic variability in the method. The adhesion test has low accuracy and repeatability even on flat, and especially on curved, surfaces."[57]. Enhancing the pull-off method with additional characterization is imperative to increasing the value of the results obtained by the method and establishing it as a more robust test method for unique applications inside and outside a lab environment.

2.3. Summary

Mechanical adhesion in modern epoxy structural coatings and methods to characterize it were reviewed and presented. It is clear from the literature that mechanical adhesion in epoxy coatings is not yet fully understood and requires more investigation. With the increase in popularity of nanomaterials in recent years, it is reasonable to assume that more materials will incorporate nanofillers because of their incredible properties and wide range of applicability. Adding nanoparticles into a polymer matrix will inevitably alter the mechanical properties of the composite coating material, and thus, the way it will fail under different loading conditions. It has been displayed that acoustic emission can be used to capture acoustic noise signals across differing adhesive failure modes in nanocomposites. This study aims to discover if the results retrieved by acoustic emission can assist in characterizing mechanical adhesion failure in epoxy-based nanocomposite coating systems and if there exist correlations that enhance the results of modern mechanical adhesion testing methods that may lack comprehensive results.

CHAPTER 3. MECHANICAL ADHESION OF STRUCTURAL POLYMER NANOCOMPOSITES AND THEIR CHARACTERIZATION METHODS

3.1. Introduction

This chapter provides fundamental concepts of mechanical adhesion in polymeric coatings, primarily focusing on epoxy-based polymer nanocomposites. Methods used to characterize adhesion and delamination are also presented to provide background on the methods used in the subsequent chapters following.

3.2. Mechanical Adhesion Mechanism of Polymer Nanocomposites

3.2.1. Substrate Adhesion in Polymeric Coatings

There are 2 primary phenomena that aim to explain a polymer's adherence to another material: (1) chemical bonding and adsorption and (2) mechanical interlocking (Fig. 3.1)[41]. Although these two phenomena are debated on which is more impactful in a coating's bond strength, it has been agreed that both interactions contribute to the adhesion strength of polymers to an extent[15], [16], [23], [41], [60]. It is noted that the acid-base theory of adhesion is a competing theory that has gained a lot of traction in recent years but lacks sufficient evidence to stand on its own as an all-encompassing theory to explain adhesion between a polymer and its substrate[23], [41]. Chemical bonding and adsorption are generally referred to as the sum of forces at the molecular level, including forces from Van der Waals interactions, hydrogen bonding, and molecular bonding (Fig. 3.2). Mechanical interlocking results from pores in the substrate getting penetrated by the liquid polymer, creating a "hook-like" structure as seen in Fig. 3.3 that mechanically entangles the two materials[15], [16], [23], [41], [60].
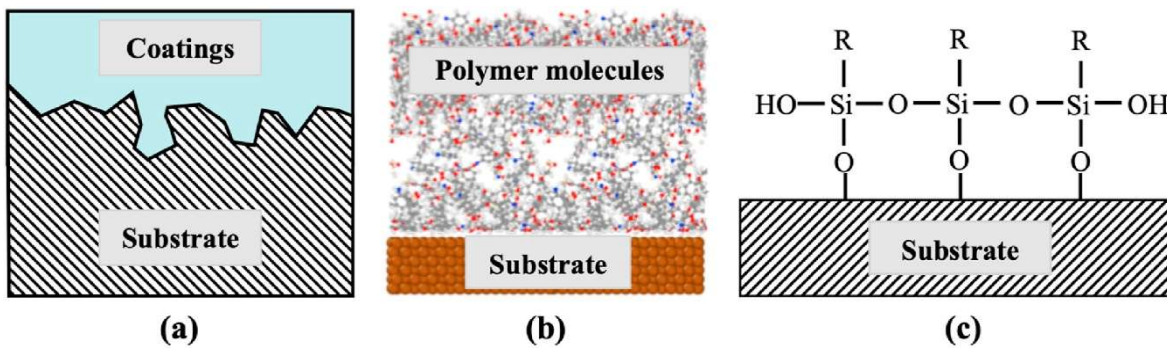
Figure 3.1: Representations of the main mechanisms that control the metal/polymer adhesion: (a) Mechanical interlocking mechanism; (b) Adsorption mechanism; (c) Chemical bonding [41]
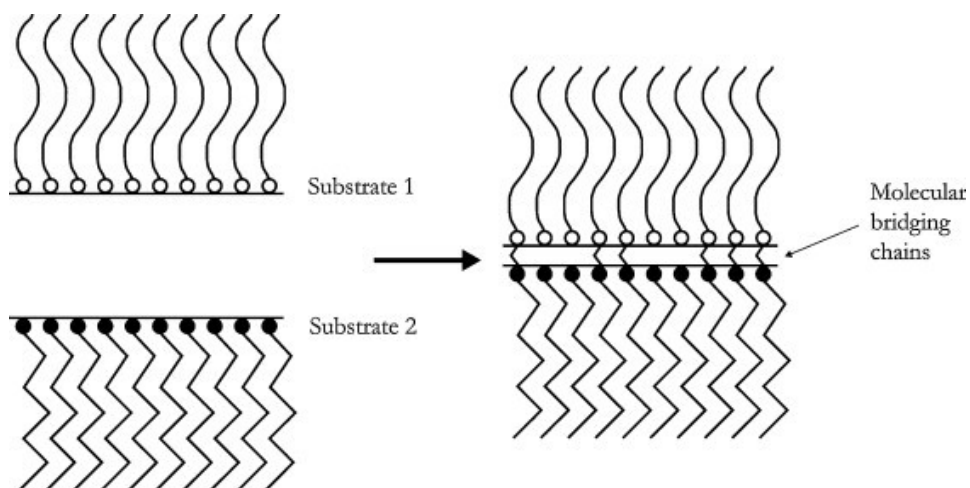
Figure 3.2: Schematic of the molecular bonding between substrates [23]
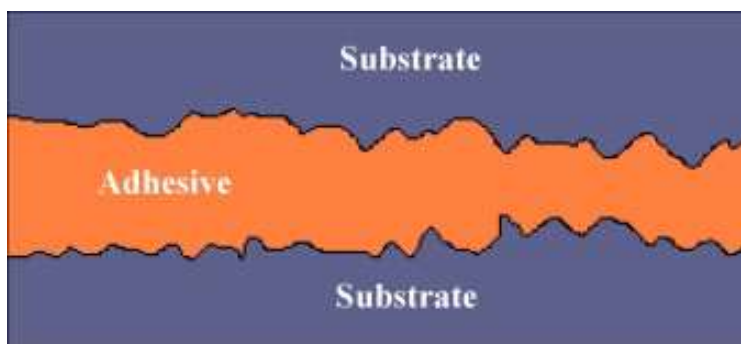
Figure 3.3: Illustration of mechanical coupling between two substrates [23]

Chemical bonds are considered a strong factor that dictate a polymer's adhesion. The formation of covalent bonds between polymers and their substrate are characterized by a high energy differential between the atoms, resulting in bond energy of 200 kJ/mol up to 900 kJ/mol[41]. Secondary bonding mechanisms resulting from the 2-phase nature in liquid polymers also help dictate its adhesive bond to its substrate. Van der Waals forces and hydrogen bonds result from intermolecular charge distribution and attraction between dipoles resulting in attractive forces between the polymer and the substrate. These forces only see bond energy between 8 kJ/mol and 42 kJ/mol in hydrogen bonds and even less in Van der Waals forces. This phenomenon is what was previously referred to as adsorption[41].

Epoxy's chemical composition is characterized by aliphatic hydroxyl and ether groups. Metal oxides present on the surface of steel substrates creates a strong electromagnetic attraction to epoxy (adsorption). The formation of chemical bonds between the active hydrogen on the steel surface and epoxide groups give a strong resulting adhesion between the two materials[15]. The discussed functional groups in a typical epoxy polymer chain are highlighted in Fig. 3.4 [61].
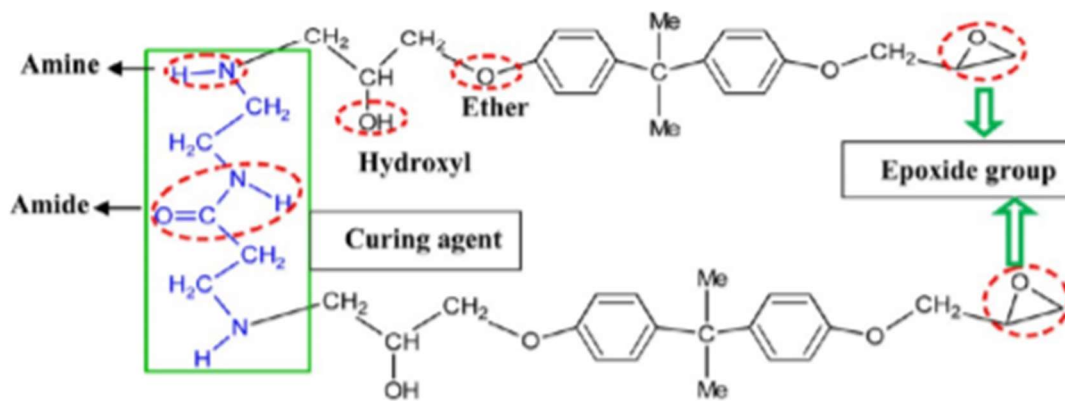
Figure 3.4: Chemical structure of aminoamide-cross-linked DGEBA epoxy resin. The functional groups were encircled by red dotted lines [61]

3.2.2. Effect of Nanomaterials on Mechanical Properties of Epoxy

There is recent literature showing the effect of adding nanoparticles to epoxy resin, remarking on the positive effects on the mechanical properties of the resulting composite material. Although they have been shown to increase cohesive and adhesive strength in epoxy coatings, there is a critical filler content limit that decreases coating strength and overall performance when passed.

Nanofillers interact with the polymer matrix at the chain interface, increasing its fracture toughness proportionately as the bond strength is increased between the resin and the filler material. If the interfacial bond between the matrix and filler material is high enough the strength experienced by the matrix will effectively transfer to the reinforcement. As in most nanofillers, the strength of the material is extremely high due to their high surface area and will effectively take much more loading on the micro and nano scales. This favorable stress distribution leads to higher strength and toughness in the bulk composite material. The addition of reinforcement medium also increases rigidity by restricting the movement of the polymer chains at the molecular level, leading to an increased stiffness[41]. Fig. 3.5 shows a schematic of the coating-filler interaction that influences a coating's cohesive strength.
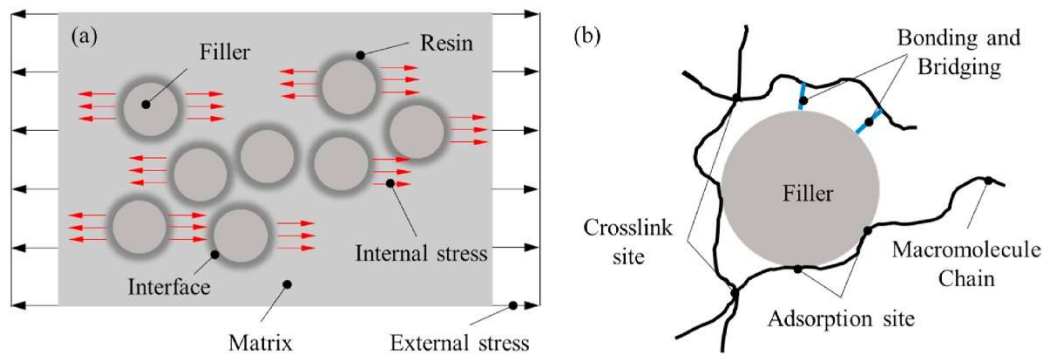
Figure 3.5: (a) Schematic model of morphological stress transformations in filled polymer matrix, and (b) Schematic model of connections between polymer chain and filler surface [41]

Additionally, the reinforcement stops microcracks from spreading. As the cracks progress, they are forced to propagate around the filler material. This is the main mechanism attributed to fracture toughness reinforcement in epoxy resin nanocomposites. Fig. 3.6 shows this phenomenon.
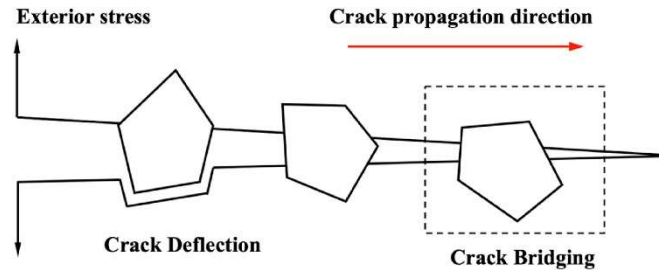
Figure 3.6: Schematic model of crack bridging and crack deflection of nanoparticles [41]

The addition of nanofillers has been shown to increase the interfacial bond strength between epoxy nanocomposites and metallic substrates. The addition of Silica (SiO_2), CNT, and GNP have all been shown to increase cohesive and adhesive strength in epoxy coatings[41]. A list of references displaying percent increase in adhesive strength of various epoxy-based nanocomposites, compiled by Wei et al., is shown in Fig. 3.7. As reinforcing nanoparticles are added, the viscosity of the resin will increase along with a decrease in its ability to wet the substrate effectively at high concentrations. These changes in physical properties of the resin before curing can severely impact the performance of the coating during its service life if the reinforcement content is set too high.

Year	Nanofiller	Content (wt.%)	Adherents	Untreated (MPa)	Treated (MPa)	Enhanced (%)	Test methods	Ref
2008	Al_2O_3	2	Steel	3.8	18.4	384	Pull off	[107]
2013	Al_2O_3	1.5	Aluminum	7.6	12.8	68	Lap shear	[106]
2016	TiO_2	10	Copper	8.7	13	72	Lap shear	[30]
2016	SiO_2	20	Stainless steel	18	21.52	20	Lap shear	[90]
2016	CNT	1	Aluminum	14	21.4	20	Lap shear	[103]
2016	RGO	0.5	Aluminum-alloy	23.82	30.06	27	Lap shear	[119]
2016	AGO	0.1	Steel	3.5	5	43	Pull off	[120]
2016	MWCNT	0.07	Mild steel	21	24	14	Lap shear	[95]
2017	CNT	5	Mild steel	1.87	3.3	76	Pull off	[98]
2017	GO + SiO_2	0.1	Mild steel	8.5	17.7	108	Pull off	[83]
2018	TiO_2	4	Stainless steel	10.56	19.74	87	Lap shear	[91]
2018	SiO_2	6	Stainless steel	10.56	20.18	91	Lap shear	[91]
2018	Al_2O_3	4	Stainless steel	10.56	20.84	97	Lap shear	[91]
2018	CNT	1	Aluminum	5.54	8.21	48	Lap shear	[96]
2018	Nano-clay	1	Aluminum	5.54	8.46	52	Lap shear	[96]
2019	Silica	3	Steel	4.98	13.88	179	Pull off	[121]
2019	Al_2O_3	5	Aluminum	6.6	10.2	55	Lap shear	[105]
2019	Al_2O_3	1	Aluminum	4.8	7.2	54	Lap shear	[104]

Figure 3.7: The effect of improvement in adhesion strengthening with respect to different filler loadings [41]

The filler content percentage is dictated by the maximum amount that can be effectively dispersed in the resin. As the reinforcement content limit is reached, the failure mode during mechanical loading will switch from a cohesive failure to an adhesive failure. This occurs due to the

27

impact of reinforcement agglomerates: bunches of nanoparticles resulting from physical and chemical attraction to each other (Fig. 3.8)[62]. The agglomerated nanoparticles that sit on the substrate will prevent the polymer chains from physically interlocking with the surface and chemically bonding to the oxide layer present on the metal which both give it its characteristic bond strength. These sites will provide a nucleation zone for interface cracks that will lead to delamination and mechanical failure.
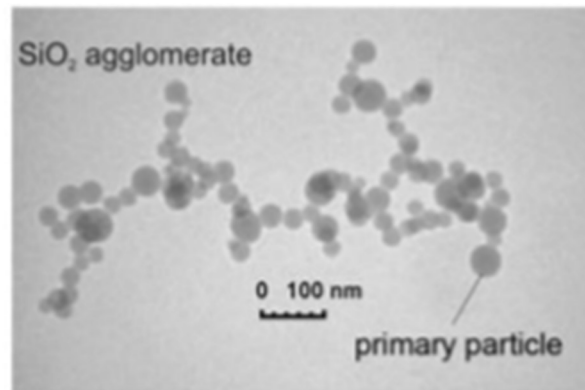
Figure 3.8: SiO_2 agglomerate[62]

There are many ways to improve particle dispersion in epoxy. One such method, ultrasonic dispersion, involves sending ultrasonic waves through the reinforced resin that induces cavitation bubbles. These bubbles will reach a critical diameter and then implode, causing "hot spots" with extremely high pressure and temperature which split up the agglomerated nanoparticles[63]. Amplitude of the waves emitted, and the time of sonication are most impactful in the ultrasonication dispersion process as shown in Fig. 3.9 [64].
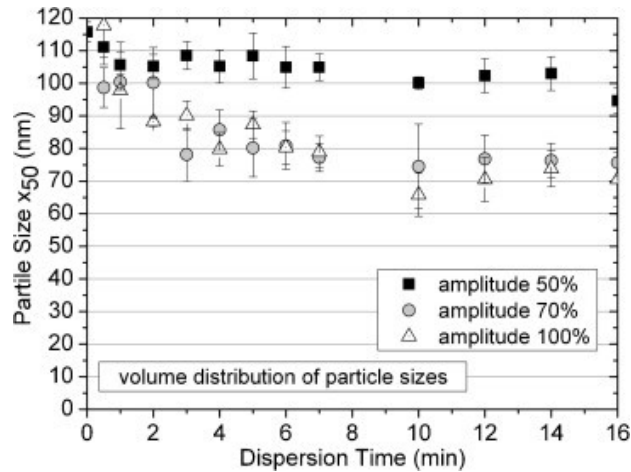
Figure 3.9: Influence of the amplitude and dispersion time on the development of the particle size[63]

3.3. Characterization Methods for Coating Adhesion

There are many ways to directly characterize the adhesion strength of coatings[15], [23], [49], [65]. Existing active and passive characterization methods are explored and explained in the following section.

3.3.1. Acoustic Emission

Acoustic emission has seen success in many industries ranging from material engineering to seismic monitoring. The principle of acoustic emission is material failures, resulting from any internal or external stimulus, will create an acoustic wave throughout the material that can be picked up by an AE sensor and analyzed by an AE system. The signals collected are referred to as transient elastic waves. Stimuli such as mechanical stress will produce acoustic waves if it causes an internal or surface failure within the structure (Fig 3.10)[46]. Modern AE systems and the data they collect are outlined in the following paragraphs.
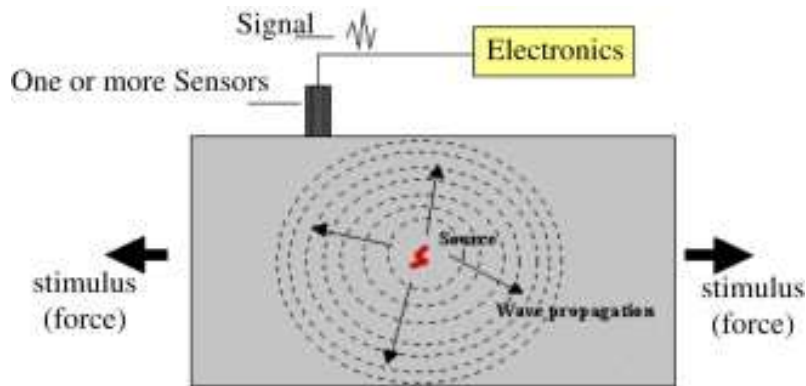
Figure 3.10: Principle of acoustic emission [46]

The typical modern acoustic emission setup consists of five components: the sensor, the preamplifier, the main amplifier with acoustic wave filters, and the data acquisition device/software (Fig. 3.11)[66]. The preamplifier is designed to help eliminate unwanted signals by supplying an adequate voltage that can provide enough gain and cable drive capability to the small AE signals. It is common to see preamplifiers installed into the sensor itself, adjacent to the transducer, instead of having a separate device wired in series like in older acoustic emission systems. Once the signal passes through the preamplifier it proceeds to another amplifier that removes maximum and minimum amplitude frequencies based on thresholds set by the user prior to testing. Finally, after all the noise filters have been passed through, the signal reaches the computer or other device used to record and analyze the data[46], [66], [67].
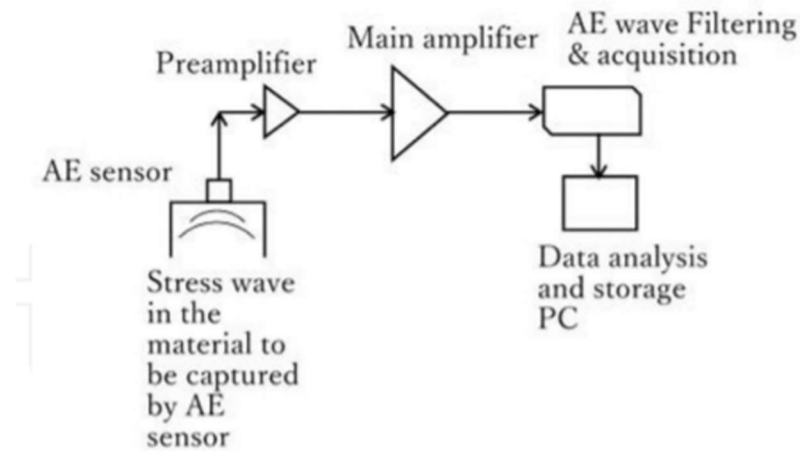
Figure 3.11: Fundamentals of AE technique [66]

The main components in a typical acoustic sensor include a bottom wear surface, the piezoelectric transducer component, and some damping material. The wear surface is meant to be in contact with the material surface and acts as a barrier between the material and the piezoelectric material in the sensor. This barrier acts to protect the sensors internal components and adequately transfer elastic waves to the piezoelectric component. The piezoelectric component experiences the acoustic waves generated by the material and converts those into electrical signals to eventually be collected and analyzed by the system. The most common piezoceramic used as the transducer is lead zirconate titanate (PZT) because of its high sensitivity, high workability, and low cost. The damping or "backing" material is designed to prevent noise echoing within the sensor housing and increase the frequency range at which the sensor can operate efficiently. A couplant is used between the wear surface and the structure's surface to avoid retarding of sound transmission between the structure or material and the sensor across air. The couplant used is based on the environment the sensor is being placed in and can be glue, grease and/or oil, ultrasound gel, or a mechanical attachment such as a weld. A visual layout of a typical AE sensor is shown in Fig. 3.12. Other sensors with rollers have also been developed for dynamic structure testing[68]–[70].
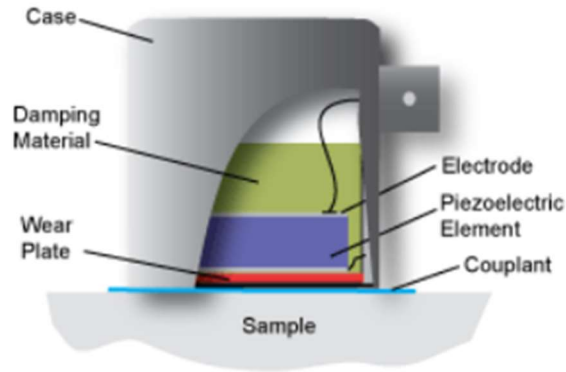
Figure 3.12: Typical acoustic sensor housing composition [70]

The sensor transducer being used is chosen based off the testing application and the type of damage the user is attempting to detect through acoustic waves. There are two main classes of transducers: resonant or broadband. Broadband sensors have the structure as described previously, with a backing material within the housing. These sensors can detect acoustic waves or a wide range of frequencies and are useful for most AE applications but are not very sensitive. Resonant sensors operate without this backing material and the main element altered to increase sensitivity is the thickness of the piezoelectric transducer. These resonant sensors provide very high sensitivity testing, with sensitivities ranging from 20-40 dB more sensitive than those in ultrasonic testing. Resonant sensors are most sensitive at their resonance frequency. Broadband sensors help to give a comprehensive picture of all acoustic waves generated within the material or structure while resonant sensors can help detect acoustic waves that would get missed by the broadband sensor because of its lack of sensitivity. To get a realistic story of what the material is experiencing, either a compromise or combination of sensitivity and broadband usually needs to be achieved[68]–[70].

Acoustic emission is most easily detected when a material undergoes plastic deformation. The "Kaiser Effect" says that a material will not produce more elastic waves unless it is loaded past the previous maximum stress that it was loaded to the first time, meaning that the acoustic waves detected

are irreversible just as plastic deformation is without some outside healing source. There are two major significances of the Kaiser Effect: (1) the highest amplitude frequency generated is at the material's yield point since so much energy gets stored in the elastic region of the stress-strain curve of the material and gets released in a short time period in the form of elastic sound waves and (2) the previous maximum loading in the material can be found very easily through AE since it will be the stress at which acoustic waves begin to generate as shown graphically in Fig. 3.13. These two conclusions combined indicate that there can be specific acoustic wave frequencies associated with specific types of plastic failure in materials[46], [66], [70], [71].

a)
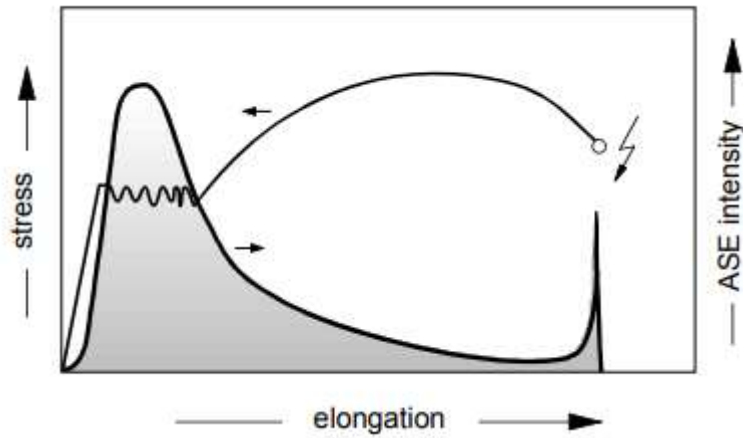
b)
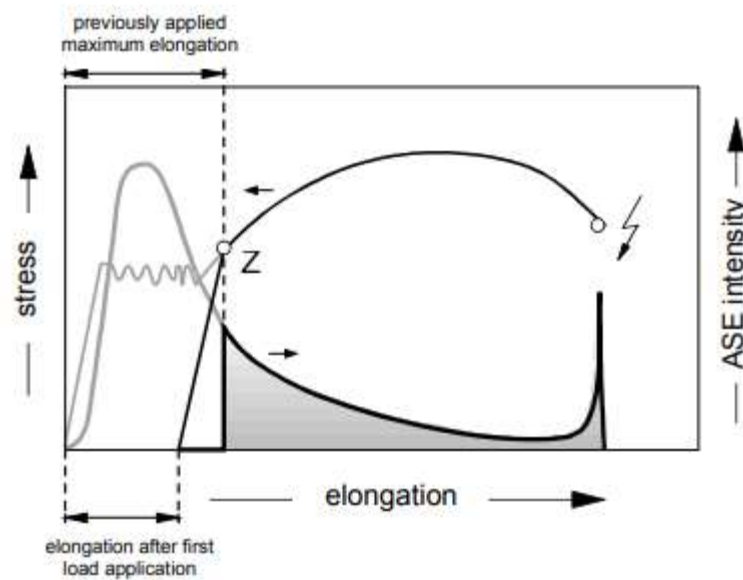
Figure 3.13: (a) Stress-strain diagram and ASE-strain diagram of a soft-annealed steel probe with 0,15 wght% carbon and (b) The KAISER EFFECT, schematics from H. M. Tensi's doctoral thesis 1960 [71]

It has been shown that composite materials do not necessarily exhibit the same effect at reloading. This is referred to as the "Felicity Effect". The ratio of the previous loading to the new loading required is called the Felicity ratio, which helps gives a more accurate representation of existing damage progression in the material. This phenomenon is illustrated in Fig. 3.14 [46].
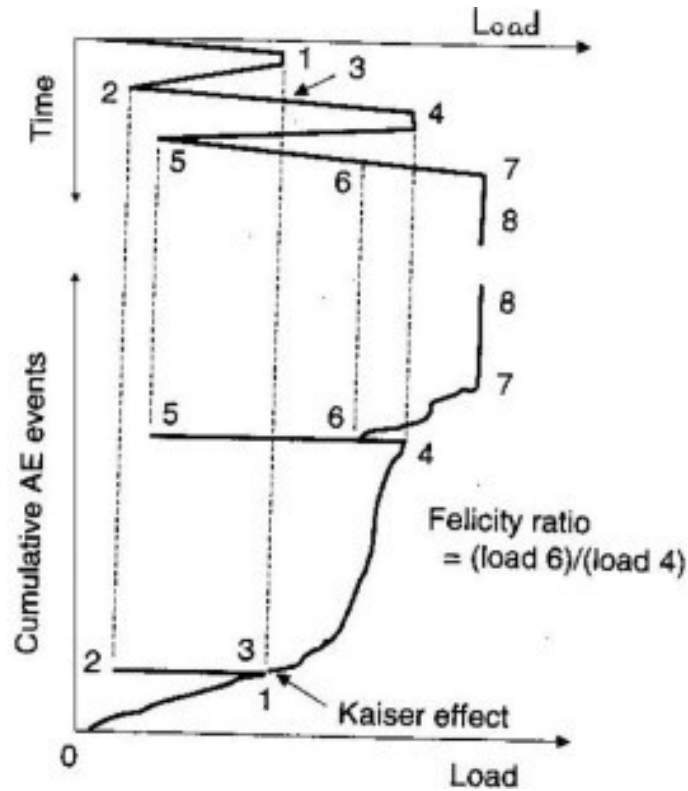
Figure 3.14: Kaiser and Felicity effects [46]

Attenuation refers to a material's level of damping of acoustic signals. As signals pass through more ductile materials, the strength of the signal diminishes over shorter distances than in brittle materials as kinetic and elastic energy is converted to thermal energy. All materials have some level of acoustic signal attenuation. The speed at which a signal travels through a material is called its wave velocity[70], [72], [73].

Wave velocity and attenuation can be obtained experimentally by the pencil-lead break test. The test requires use of a tool known as a Hsu-Nielson Source. The test consists of breaking pencil lead against the structure by using a mechanical pencil with 0.3 or 0.5 mm 2H lead with a cone-shaped shoe designed to make the lead break at a 30-degree angle repeatably. The signal generated by the lead breaking is relatively consistent and repeatable and can be conducted at different distances to measure wave velocity and attenuation of the material being tested[72], [73].

There are several significant parameters to consider when looking at collected AE data. The primary characteristics of an acoustic event analyzed are hits, rise time, amplitude, and counts. An acoustic event is a comprehensive representation of the acoustic wave during the testing period. It works best to consider events relative to location within the material since they just indicate where acoustic hits have taken place as opposed to the severity or amplitude of that acoustic signal. Acoustic emission events can be compromised of one or many acoustic hits from multiple different sensors on the same structure or material. An acoustic hit refers to any signal that passes above the user-defined frequency threshold. Hits can be analyzed individually by looking at their amplitude, rise time, and duration to further explain the acoustic wave collected. A "count" refers to a wavelength passing over the threshold with each hit usually consisting of many counts. The amplitude of the wave indicates how far above the threshold the count passed. Fig. 3.15 shows a basic acoustic event[46], [66], [69], [70].
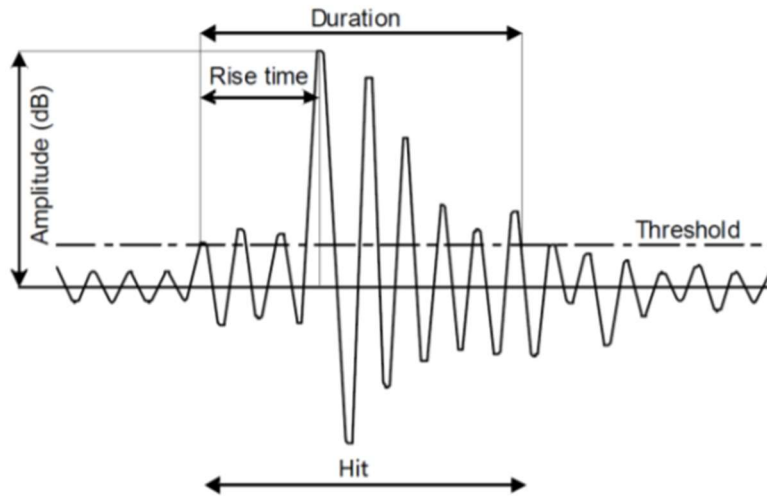
Figure 3.15: Diagram of hit definition [69]

3.3.2. ASTM D4541 Pull-Off Test

The stud/butt test, or more generally referred to as the pull-off test, involves applying an adhesive to a metallic stud which is adhered to the surface of the sample and then removed via force applied perpendicular to the surface of the substrate[23]. A simple schematic diagram of the general test is shown in Fig 3.16.
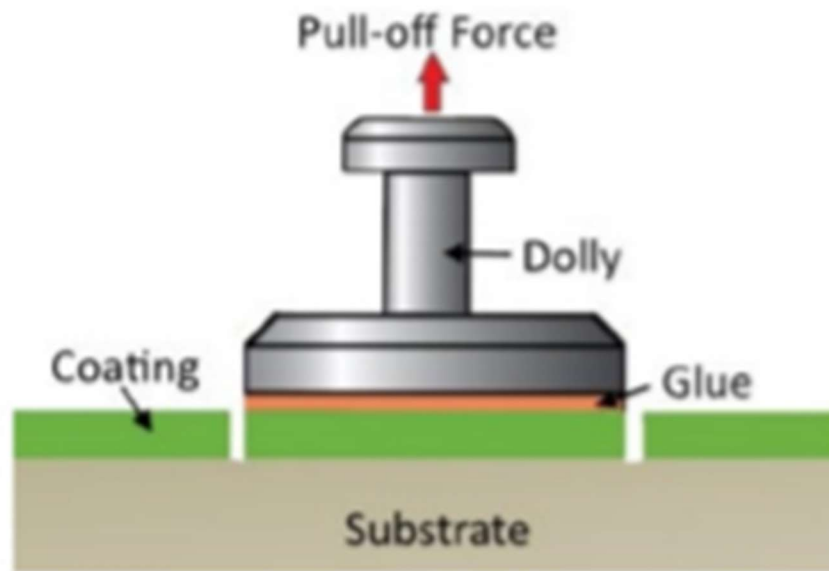
Figure 3.16: ASTM D4541 Pull-Off test schematic [52]

ASTM details a widely used standard for conducting the pull-off test and reporting results obtained from it. The standard testing procedure provided serves as a guide to uniformly preparing and testing samples. The test has two protocols it can be reasonably used for: (1) test to fracture or (2) pass/fail. A flow chart for the two testing procedures is provided in Fig. 3.17. The inconsistencies in coating adhesion between tests require variability tolerances for acceptable reporting data. Precision tests were conducted on 7 different coatings with 5 different testing apparatus by ASTM in 2006. Coatings B through E are reported with averages testing apparatus B-F. Coatings A and F surpassed

the capacities of several of the testing apparatus. Acceptable variabilities found are shown in Fig. 3.18[58].
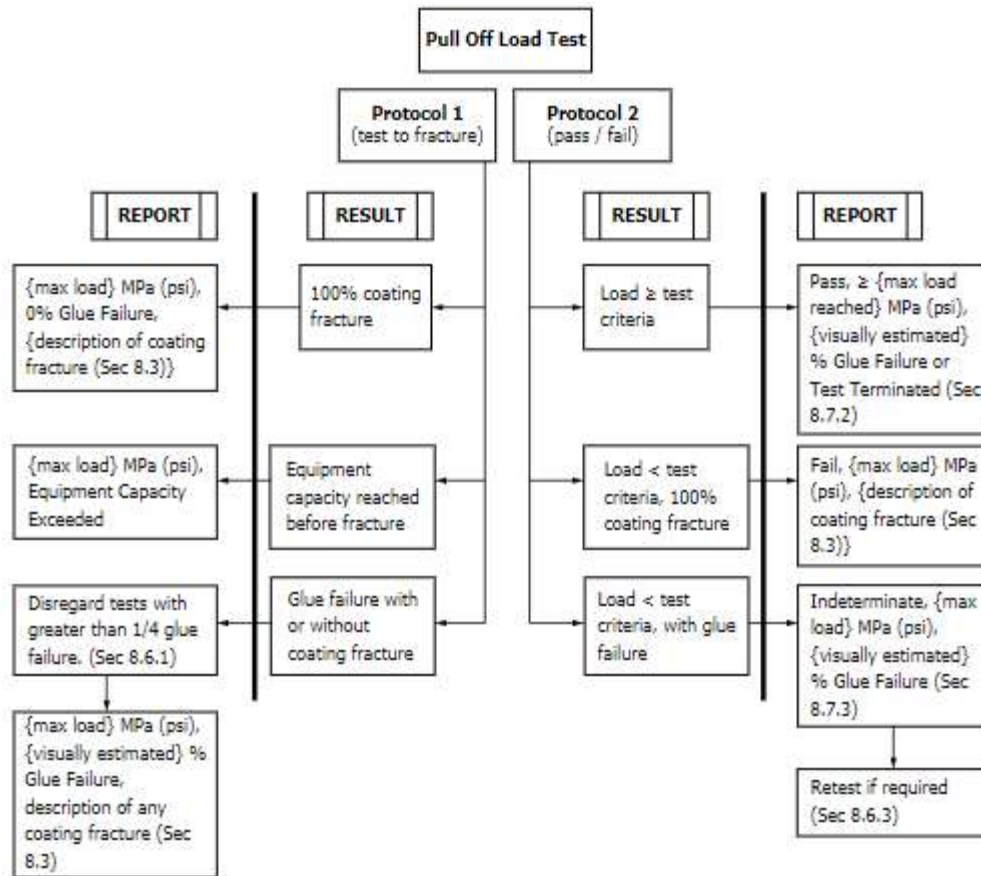
Figure 3.17: ASTM D4541 flow chart [74]

Intralaboratory	Maximum Recommended Difference, %	Interlaboratory	Maximum Recommended Difference, %
Method B	64.7	Method B	76.0
Method C	33.8	Method C	65.9
Method D	14.8	Method D	28.4
Method E	27.8	Method E	34.1
Method F	17.5	Method F	23.0

Figure 3.18: Precision of Adhesion Pull-Off Measurements (averaged across coating types for each instrument)[74]

CHAPTER 4. EXPERIMENTAL METHODOLOGY

4.1. Introduction

This chapter presents the experimental procedures used to study mechanical delamination in epoxy-based nanocomposites. Acoustic emission in conjunction with a modified pull-off test was used to investigate the phenomena present during mechanical delamination. Imaging was used following the testing to assist in analysis of the results. The following sections outline the details of the testing methods.

4.2. Experimental Plan

As stated in objective 3 in Chapter 1, epoxy mixed with 3 different nanoparticles at 2 different thicknesses will be tested to explore relationships between the coating systems. In an effort to explore objective 1 outlined in Chapter 1, A tensile testing machine will be used to rip off dollies glued to the coating while acoustic sensors capture the noise generated before and during failure in the coating. Following the testing, imaging will be conducted on the tested areas to fulfill objective 2 in Chapter 1.

4.3. Material Preparation

The experimental plan aims to explore three different epoxy-based polymer nanocomposite coating systems on steel. The three different nanoparticles used were silica, CNTs, and GNPs. The wet epoxy nanocomposite solution was applied at thicknesses of 4 and 8 mils. The coatings were cast on 6"x12"x0.032" steel panels following a rigorous dispersion process.

4.3.1. Material Properties

EPON™ Resin 828 was used as the bisphenol A epoxy resin and the curing agent used was Epikure 3175; the resin and curing agent used were obtained from Hexion Inc. (Columbus, OH, USA). Silicon Dioxide was obtained from Sigma-Aldrich (St. Louis, MO, USA). The particle size was 10-20

nm. The multi-walled carbon nanotubes and graphene were both obtained from Cheap Tubes Inc. (Cambridgeport, VT, USA). The length of the CNTs was around 10-50 μm with an outer diameter of 8-15 nm. The GNPs had an average thickness of 8-12 nm. All of the materials were used as received without further chemical or surface modification.

4.3.2. Coating Mixing and Fabrication

The nanoparticles were first dispersed into the epoxy resin at a weight content ratio of 1% using a high-speed disk (HSD) disperser for 30 minutes at 4000 rpm while submerged in an ice/water bath. Next, the resin/nanoparticle slurry was subjected to an ultrasonication regiment. A ¾" sonication probe was used to agitate the slurry for 60 minutes while using a 15 second on/off cycle at 100 amps. The heat generated by the sonication required the sample to be submerged in an ice/water bath that was switched out every 15 minutes during sonication. The slurry was then mixed via mechanical stirrer with the curing agent at a ratio of 65:35 (epoxy:curing agent) for 10 minutes at a rotational speed of 600 rpm. The coatings were applied to S-612 steel panels (Q-Lab Corp., Cleveland, OH, USA) using a drawdown bar. The thicknesses applied were 4-mils (101.6 μm) and 8-mils (203.2 μm). The coatings were left to cure for 24 hours at room temperature. The measured post-cure thickness of the coatings was approximately 87±10 μm and 171±10 μm for 4 and 8 mil thicknesses, respectively.

3M™ Scotch-Weld™ Series DP460 2-part epoxy adhesive was used to attach 14 mm aluminum dollies (Fig 4.1) to the coatings following fabrication. The glue was allowed to cure for at least 24 hours before testing as per manufacturer's recommendation. Once the adhesive had had time to cure, a scoring tool was used to separate the surrounding coating from the tested area prior to testing. A picture of a prepared sample is provided in Fig. 4.2.
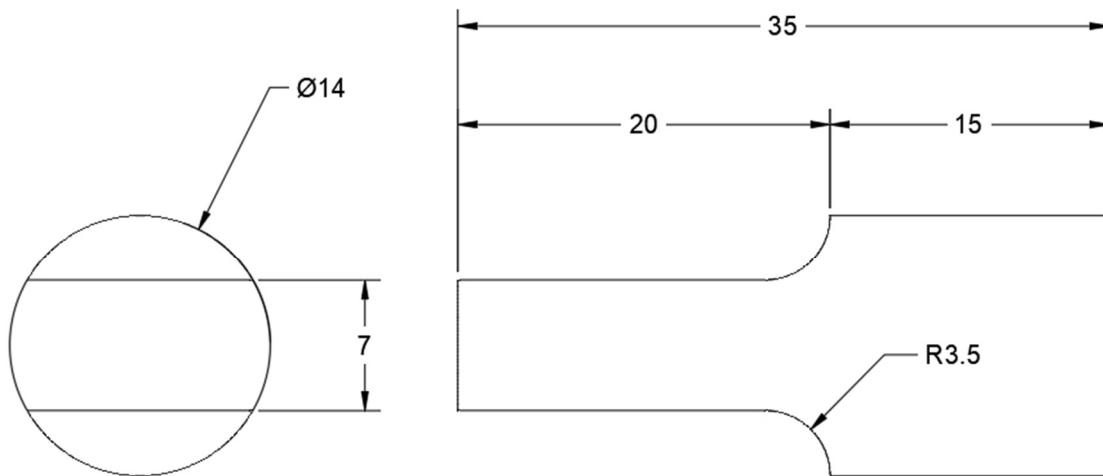
Figure 4.1: Schematic drawing of modified aluminum dolly (dimensions in mm)

Figure 4.2: Prepared sample

4.4. Testing Setup and Instrumentation

The samples were braced to a large steel weight beneath the tensile machine using 2"x1/2"x1' steel bars and C-clamps to ensure no deflection in the steel substrate during testing. A Shimadzu EZ-X Tester (Columbia, MD, USA) was used to mechanically load the specimens at an increasing rate of 0.25 lb/s (approx. 1 psi/s) until failure between the coating and the substrate occurred.

An Aewinn Micro-II Express system with R6I-AST sensor, with 40 dB integral preamplifier and internal noise filter, (Physical Acoustics Corporation, Princeton, NJ, USA) was used to capture the AE signals. The sensor has high sensitivity, with a bandwidth of 1-100 kHz and a resonance frequency of 60 kHz (Fig. 4.3). The sensor was placed 2 inches from the testing location on the steel panel and fastened with pressure tape. Acoustic couplant gel was applied before sensor placement to encourage the transfer of the acoustic signals. Pre-amp and threshold values were both set at 40 dB. PLB tests were conducted to verify the integrity of the sensors used. A picture of the final setup is shown in Fig 4.4.

Figure 4.3: Sensor used during the mechanical testing phase
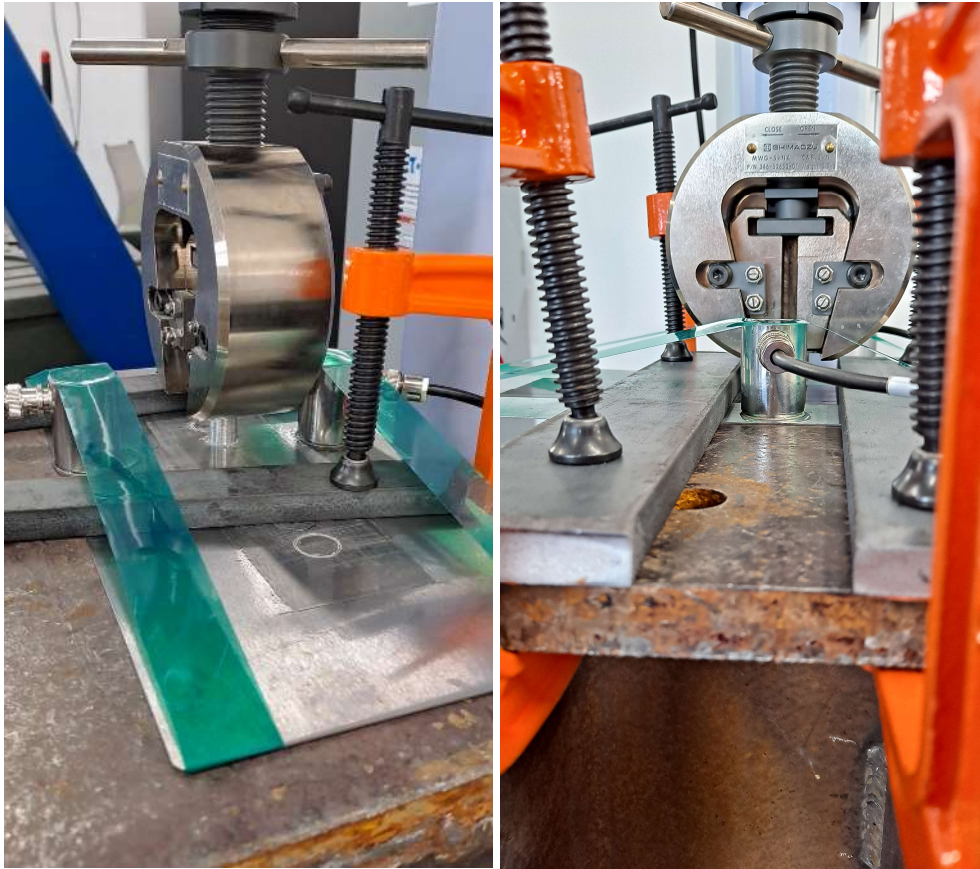
Figure 4.4: Final tensile machine setup side view (left) and front view (right).

Following the failure of the loaded samples, the setup was disassembled, and the failure area was examined. Pictures of the failures were taken by microscope for further analysis. ImageJ software was used to quantify and distinguish specific failure areas present in the pictures taken. The collected acoustic data was analyzed via Noesis, an acoustic analysis program provided by Phsyical Acoustics Corporation.

CHAPTER 5. CHARACTERIZATION OF MECHANICAL ADHESION FAILURE OF EPOXY NANOCOMPOSITES

5.1. Introduction

This chapter will outline the results obtained from eight different epoxy nanocomposite coating systems during mechanical testing, utilizing acoustic emission and post-failure, utilizing imaging software. The sample nomenclature follows the following structure:

For the sample: **E02-3**

1. E corresponds to neat epoxy. C, G, and S correspond to CNT, GNP, and Silica, respectively.

2. The "0" following the "E" corresponds to a 4-mil coating thickness. A "2" following the letter designates a coating thickness of 8-mil.

3. The last two digits surrounding the "-"(2-3 in this case) simply refers to the sample and test number and carry no other significance.

5.2. Adhesion Strength of Epoxy Nanocomposites

5.2.1. Modified ASTM D4541 Pull-Off Test

As stated prior, ASTM outlines a standardized method for the testing mechanical adhesion strength between a coating and its substrate[74]. The dollies, glue, and sample preparation all followed the specifications set by ASTM. The following were modified to accommodate this research:

1. The loading rate was set at 0.25 lb/s to main a constant stress rate across the different samples, instead of imposing a strain rate that would have inevitably changed across tests due to the varying levels of material ductility across the various modified samples. A slower loading rate allowed for more data collection

(by AE) across the more prolonged failure times of approximately 180-300 seconds (instead of the 100 second maximum set by ASTM).

2. A tensile testing machine (not approved according to the standard) was deemed acceptable to be used to achieve a controllable and precise loading rate during testing.

3. The reported area results were measured by ImageJ software instead of visual estimation.

5.2.2. Adhesion Strength Across Different Coating Systems

Fig. 5.1 shows the load data and modified load data for the samples and Table 5.1 shows the data table with values. The loading needs to be modified in all samples that do not exhibit a complete coating-substrate adhesion failure at the end of the test as specified by ASTM. The modified load value gives a more accurate representation of the coating's adhesion strength. The equation (5.1) for calculating the modified load is:

$$\text{Modified Load (psi)} = \text{Final Load (psi)} / \text{Adhesion Area (\%)} \qquad (5.1)$$
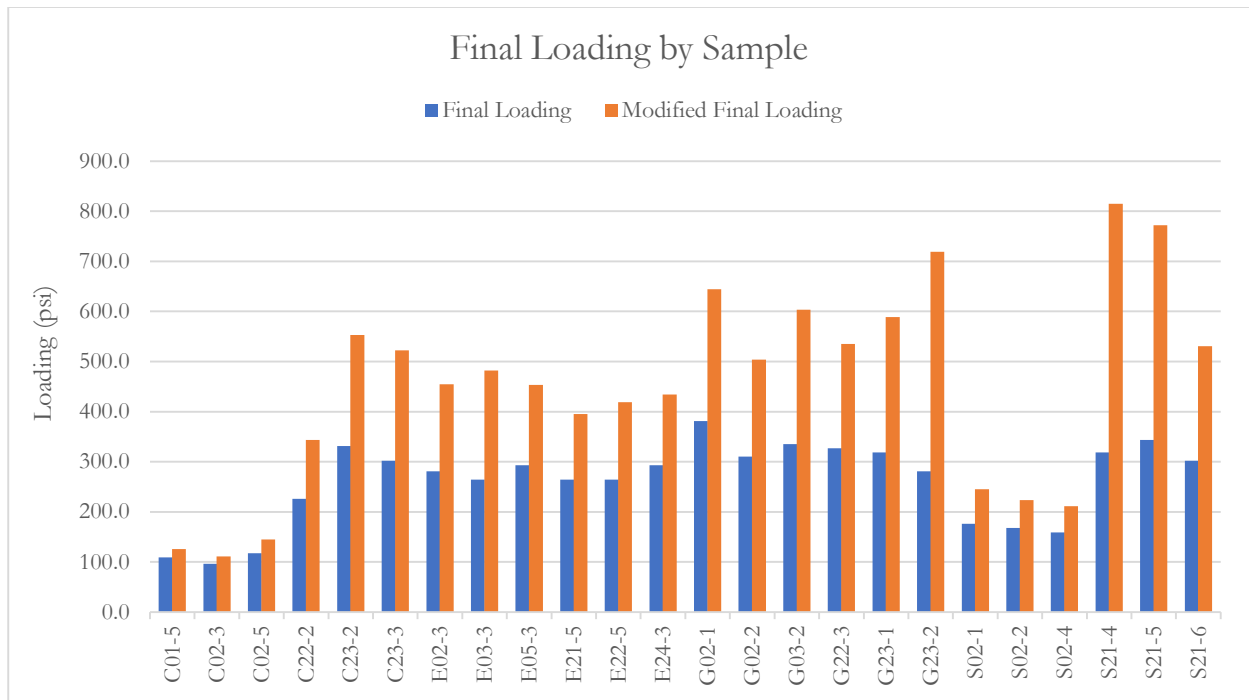
Figure 5.1: Final loading and modified final loading of all samples.

Table 5.1: Final Loading Data

Sample	Final Psi	Modified Psi
E02-3	280.8	454.88
E03-3	264.0	481.90
E05-3	293.4	453.16
Avg.	**279.4**	**463.3**
E21-5	264.0	395.14
E22-5	264.0	419.10
E24-3	293.4	434.24
Avg.	**273.8**	**416.2**
C01-5	109.0	125.84
C02-3	96.4	110.98
C02-5	117.3	144.98
Avg.	**107.6**	**127.3**
C22-2	226.3	343.32
C23-2	331.1	552.65
C23-3	301.8	522.52
Avg.	**286.4**	**472.8**
G02-1	381.4	644.56
G02-2	310.1	503.96
G03-2	335.3	603.68
Avg.	**342.3**	**584.1**
G22-3	326.9	534.85
G23-1	318.5	588.87
G23-2	280.8	718.71
Avg.	**308.7**	**614.1**
S02-1	176.0	245.09
S02-2	167.6	223.22
S02-4	159.3	211.64
Avg.	**167.6**	**226.7**
S21-4	318.5	814.42
S21-5	343.7	772.11
S21-6	301.8	530.32
Avg.	**321.3**	**705.6**

Nanoparticles were shown to increase the adhesion strength in most samples compared to the neat epoxy. Exceptions exist primarily in the CNT and Silica 4 mil samples, indicating that the agglomerates present in the coating severely impact its adhesion strength at low thicknesses. Fig. 5.2 displays a typical CNT surface with numerous agglomerates present. GNP samples did not exhibit the same behavior.

Figure 5.2: Visible agglomerates present in the CNT samples (sample shown is intentionally abraded)

5.2.3. Adhesion, Cohesion, and Glue Failure Areas

According to the ASTM standard, different failure areas in each tested area need to be quantified in terms of a percentage. The failure areas are separated into adhesion, cohesion, and glue failure. Adhesion is typically the desirable failure mechanism, which occurs between the coating and the substrate. Cohesion failures occur within the coating layer. Glue failures are the least desirable and happen between the coating and the glue or within the glue layer itself. Following testing, images of the samples were taken using a live-video microscope. The original images are reported in Fig. 5.3.
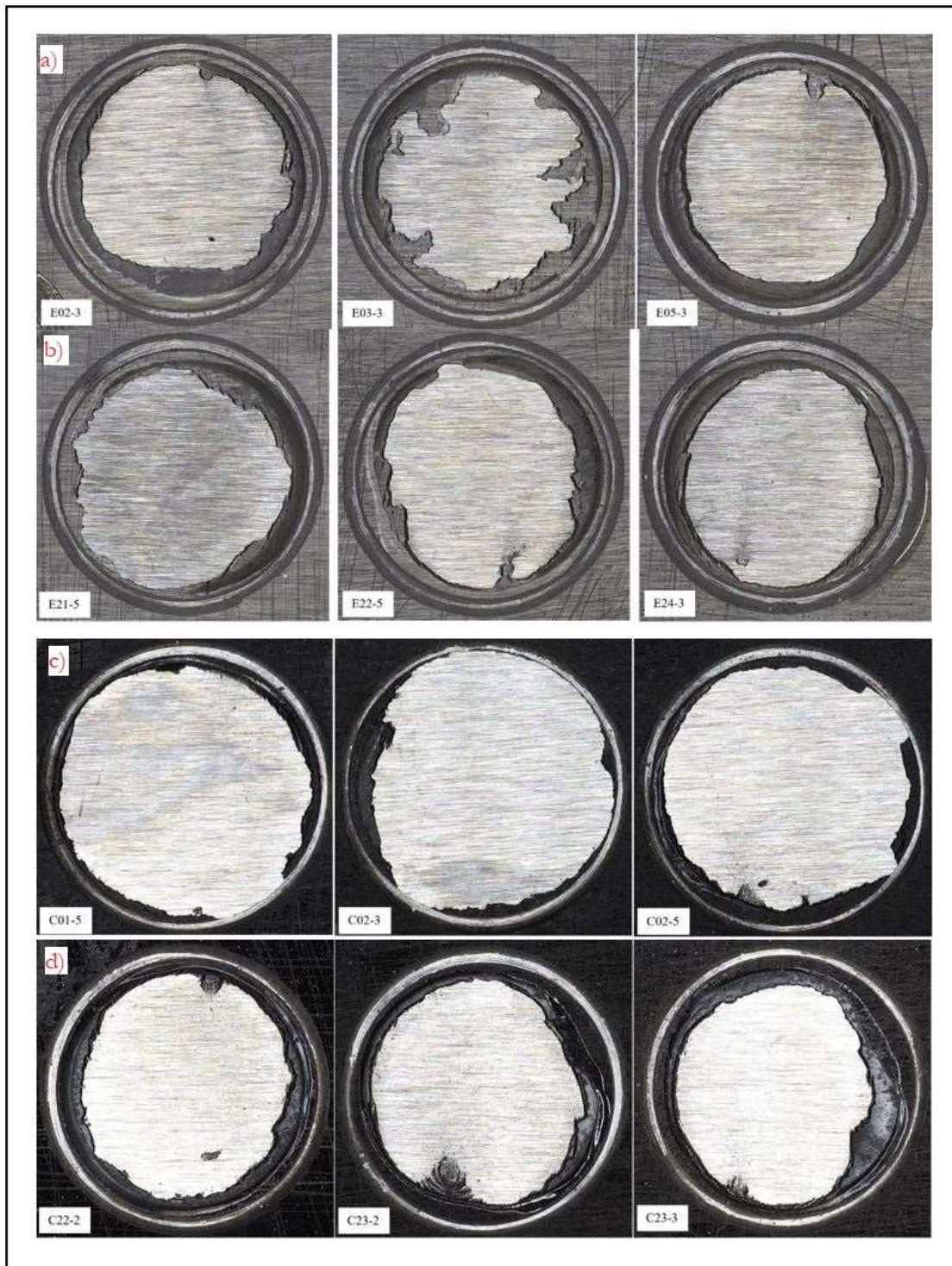
Figure 5.3: (a) 4-mil neat epoxy samples, (b) 8-mil neat epoxy samples, (c) 4-mil CNT samples, (d) 8-mil CNT samples, (e) 4-mil GNP samples, (f) 8-mil GNP samples, (g) 4-mil Silica samples, and (h) 8-mil Silica.
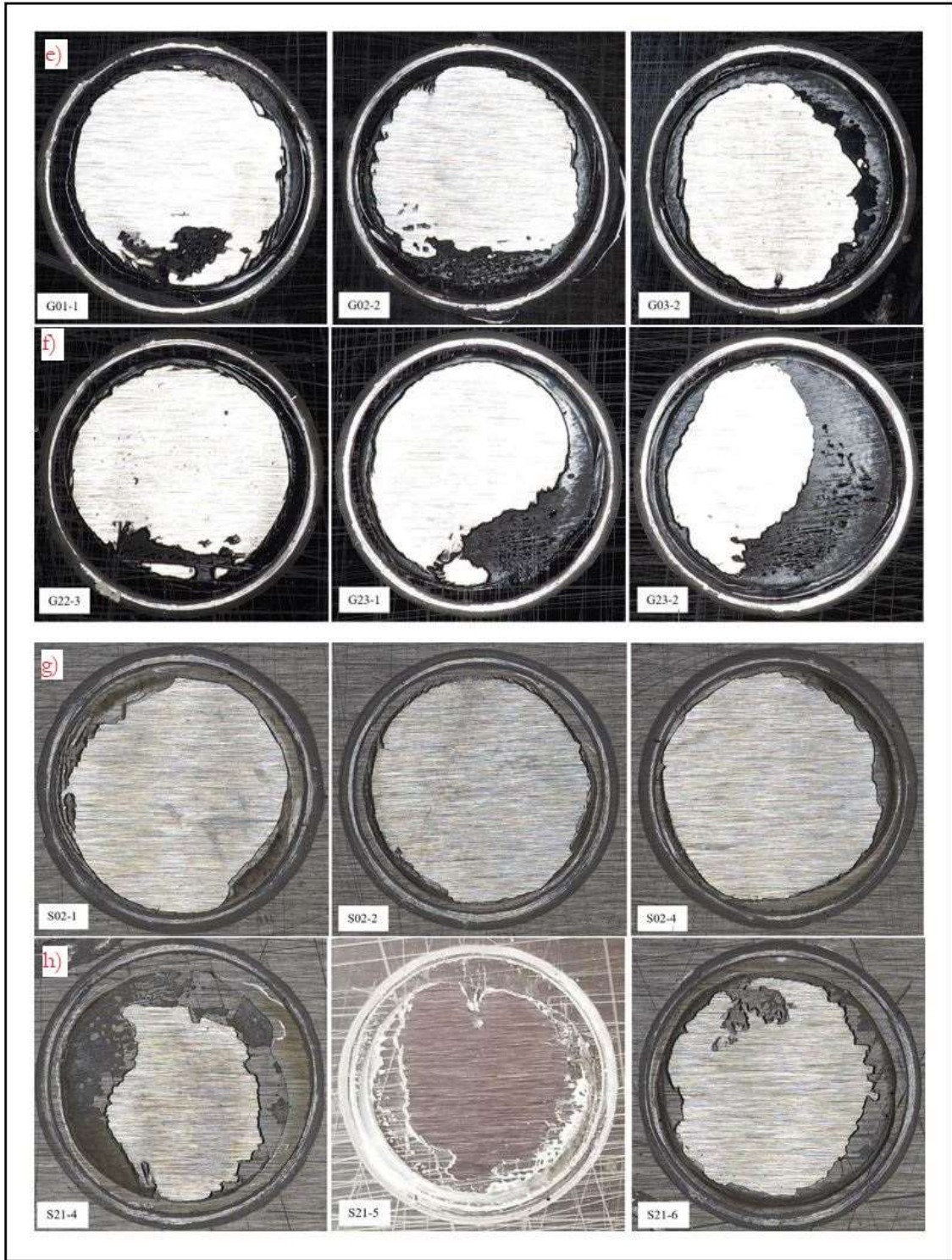
Figure 5.3: (a) 4-mil neat epoxy samples, (b) 8-mil neat epoxy samples, (c) 4-mil CNT samples, (d) 8-mil CNT samples (e) 4-mil GNP samples, (f) 8-mil GNP samples, (g) 4-mil Silica samples, and (h) 8-mil Silica samples (continued).

ImageJ software (downloaded from https://imagej.nih.gov/ij/) was used to quantify the areas more precisely on the images. The cohesion failure edges (cyan), and glue failure areas (green) were obtained via the software and overlayed to create the images seen in Figure 5.4. The resulting areas were calculated using ImageJ and are shown in Fig. 5.5. Furthermore, the area percentage breakdown for each sample is shown in Table 5.2 along with averages across sample sets. It can be seen from the data that the thicker coatings modified with nanoparticles had more cohesive failures than the thinner coatings modified with the same reinforcement but the same cannot be said for neat epoxy. 8-mil graphene displayed high values of cohesion failure whereas 8-mil silica saw very high levels of glue failure.
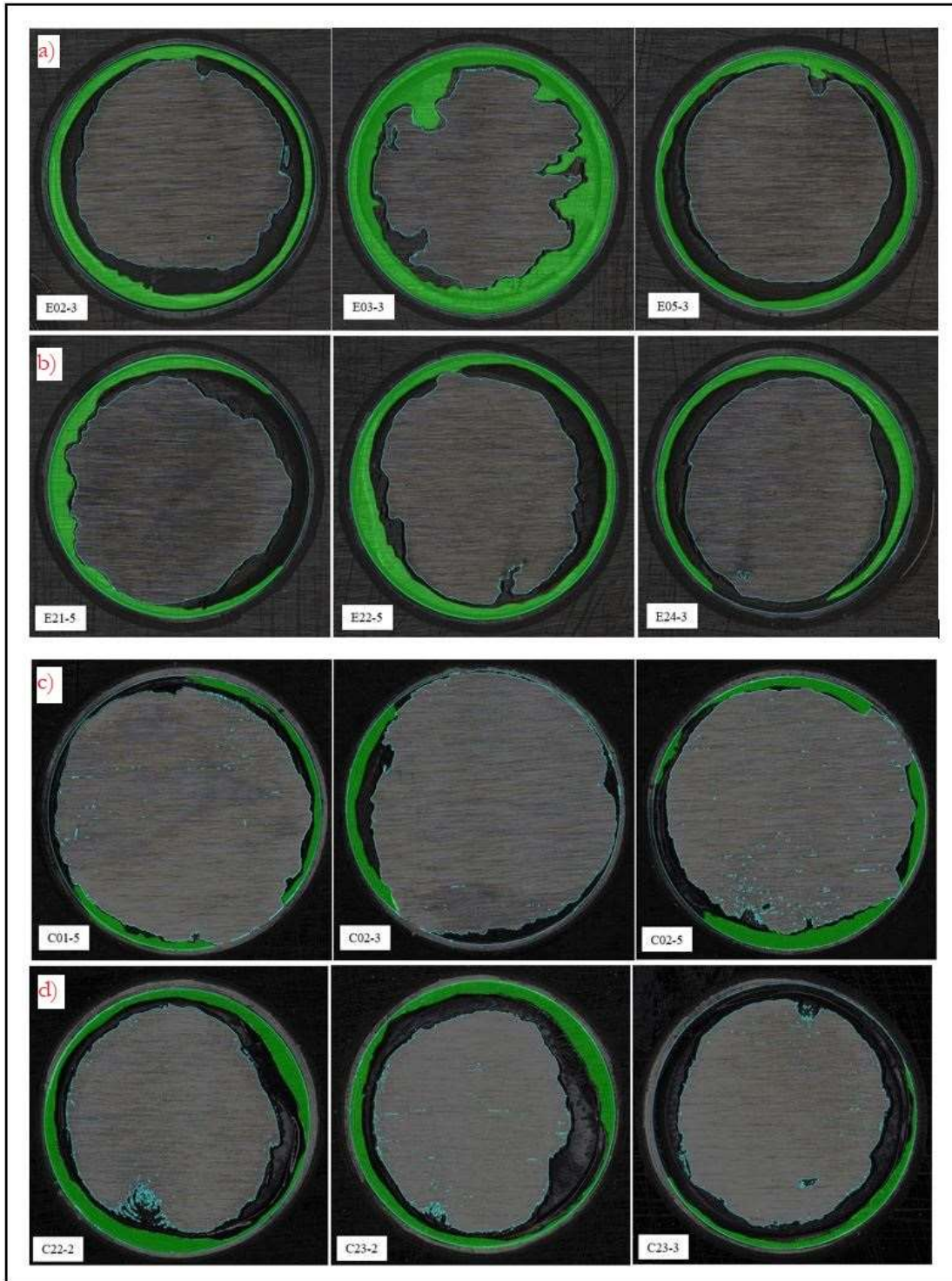
Figure 5.4: (a) 4-mil neat epoxy samples, (b) 8-mil neat epoxy samples, (c) 4-mil CNT samples, (d) 8-mil CNT samples, (e) 4-mil GNP samples, (f) 8-mil GNP samples, (g) 4-mil Silica samples, and (h) 8-mil Silica samples after ImageJ area analysis.
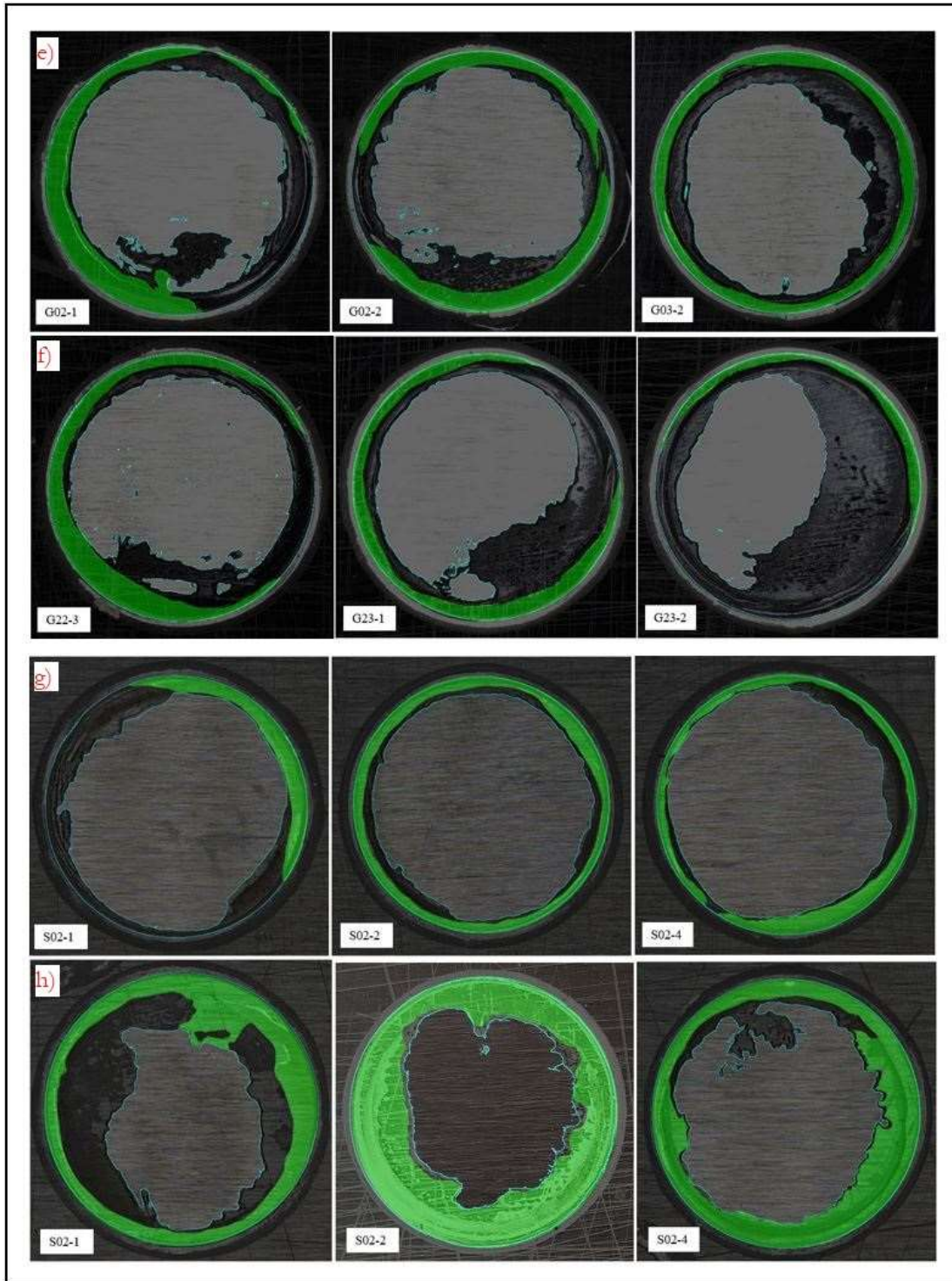
Figure 5.4: (a) 4-mil neat epoxy samples, (b) 8-mil neat epoxy samples, (c) 4-mil CNT samples, (d) 8-mil CNT samples, (e) 4-mil GNP samples, (f) 8-mil GNP samples, (g) 4-mil Silica samples, and (h) 8-mil Silica samples after ImageJ area analysis (continued).
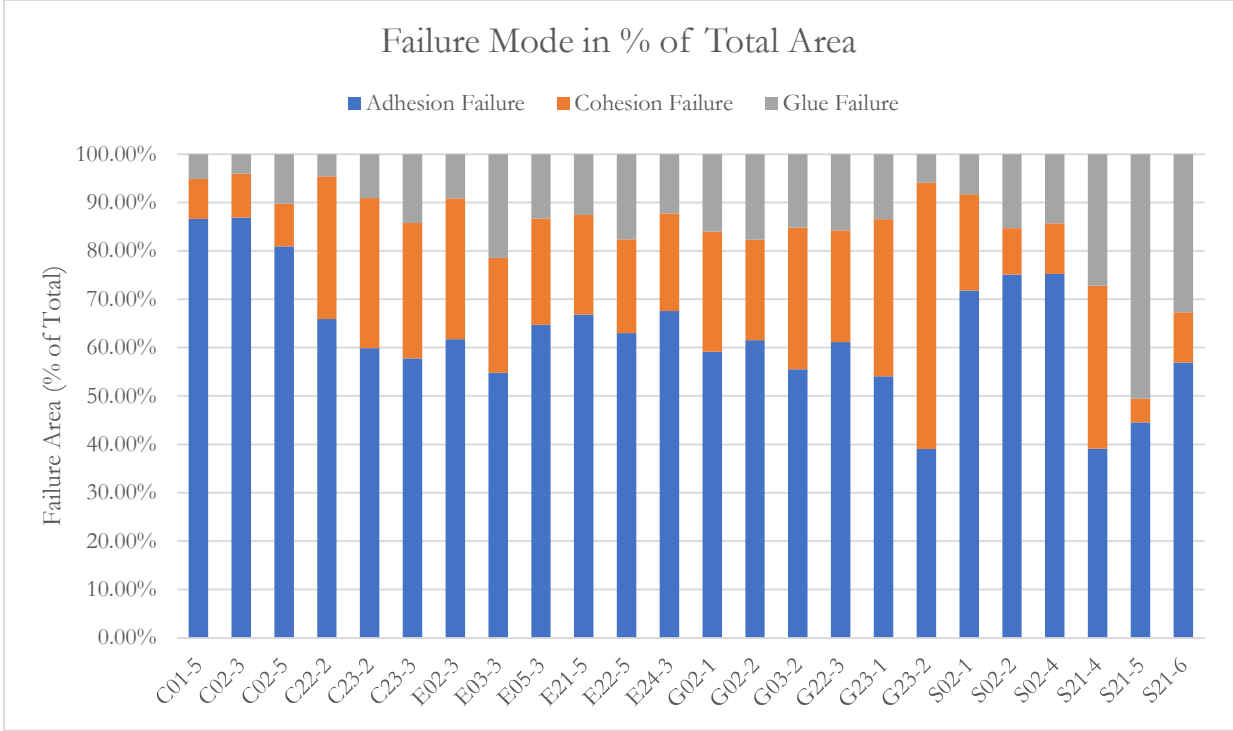
Figure 5.5: Failure areas by percentage of total tested area.

Table 5.2: Failure Areas by % of Total Area, Calculated by ImageJ Software

Sample	% Adhes.	% Cohes.	% Glue
E02-3	61.73%	29.10%	9.17%
E03-3	54.79%	23.75%	21.46%
E05-3	64.74%	21.95%	13.31%
Avg.	**60.42%**	**24.93%**	**14.65%**
E21-5	66.82%	20.57%	12.61%
E22-5	63.00%	19.36%	17.64%
E24-3	67.56%	20.18%	12.26%
Avg.	**65.79%**	**20.04%**	**14.17%**
C01-5	86.59%	8.28%	5.13%
C02-3	86.86%	9.09%	4.05%
C02-5	80.94%	8.82%	10.24%
Avg.	**84.80%**	**8.73%**	**6.47%**
C22-2	65.92%	29.49%	4.59%
C23-2	59.91%	31.00%	9.09%
C23-3	57.75%	27.98%	14.27%
Avg.	**61.19%**	**29.49%**	**9.32%**
G02-1	59.17%	24.78%	16.05%
G02-2	61.54%	20.79%	17.67%
G03-2	55.54%	29.25%	15.21%
Avg.	**58.75%**	**24.94%**	**16.31%**
G22-3	61.12%	23.09%	15.79%
G23-1	54.09%	32.48%	13.43%
G23-2	39.07%	55.03%	5.90%
Avg.	**51.43%**	**36.87%**	**11.71%**
S02-1	71.82%	19.89%	8.29%
S02-2	75.10%	9.61%	15.29%
S02-4	75.25%	10.46%	14.29%
Avg.	**74.06%**	**13.32%**	**12.62%**
S21-4	39.11%	33.69%	27.20%
S21-5	44.51%	4.94%	50.55%
S21-6	56.90%	10.38%	32.72%
Avg.	**46.84%**	**16.34%**	**36.82%**

5.2.4. Summary of Adhesion Strength of Epoxy Nanocomposites

The research verifies literature review indicating that nanoparticles reinforcement does increase mechanical adhesion strength in epoxy nanocomposites. Although the adhesion strength of the coating suffers at low thicknesses in epoxy nanocomposites due to agglomerates, it is shown that the two-dimensional nanoparticle (GNP in this case) agglomerates have less negative impact on the adhesion performance. Additionally, the neat epoxy experienced a significant decrease in adhesion performance when the thickness was increased.

As the coating thickness increases, so does its tendency towards cohesive failure when reinforced with nanoparticles. The cohesion failure area increased across all samples besides neat epoxy as the thickness was increased. It is clear based on observations that the cohesive strength gained from the reinforcement as the coating thickness is increased, enhances the coating's adhesive strength as well, preventing more areas from delaminating under applied loading (see Table 5.1 and Fig. 5.4).

5.3. Acoustic Emission Used as Adhesion Failure Characterization

5.3.1. Acoustic Emission Data Received from Mechanical Loading Failures

Acoustic sensors were attached to the samples during testing to collect the noise generated throughout the adhesion failure to characterize the different failure modes between samples and nanocomposite coating systems. The cumulative energy, cumulative AE counts, and displacement curve were plotted on the same graph as seen in Fig. 5.6-5.9. Fig. 10 shows what is referred to as the "yield point".

Observations are made among sample groups:

1. Neat Epoxy

   a. 4-mil neat epoxy samples experience acoustic events near the yield point of the material as the loading curve changes direction dramatically.

   b. 8-mil neat epoxy samples exhibit smoother curve transitions as they begin to yield and produce a significantly smaller volume of signals compared to 4-mil epoxy but produce much greater signals at failure.

2. CNT

   a. 4-mil CNT samples fail at very low loadings due to the nature of the agglomerates and produce little acoustic energy below their yield point and fail abruptly as they start to yield, resulting in a large final signal.

   b. 8-mil CNT samples produce significantly more acoustic events during testing prior to failure and have an extended period of yielding compared to 4-mil CNT. The signals produced have fewer counts, but more energy on average.

3. GNP

a. 4-mil GNP samples show low volume of acoustic events leading up to failure.

b. 8-mil GNP samples show higher volume of acoustic events prior to failure than 4-mil GNP and have lower final signals.

4. Silica

a. Like 4-mil CNT, 4-mil silica samples have low adhesion capacity and do not exhibit a yield point. Unlike CNT 4-mil, they experience a high volume of acoustic events prior to yielding and failure.

b. 8-mil silica samples show a much more defined yield point compared to 4-mil silica and experience a larger volume of acoustic events before yielding and failure than 4-mil silica.
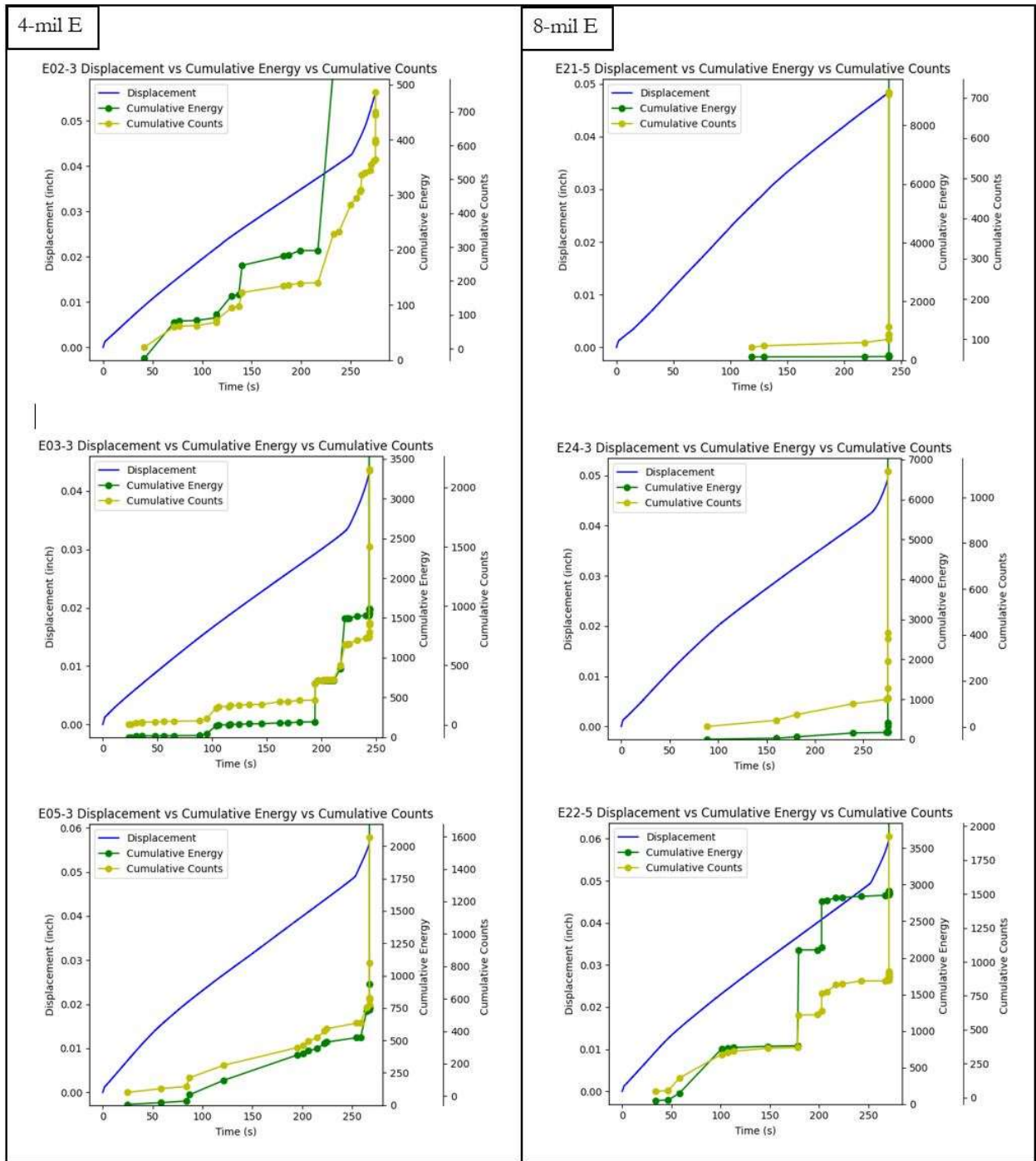
Figure 5.6: Displacement, cumulative energy, and cumulative count curves overlayed for neat epoxy 4-mil and 8-mil
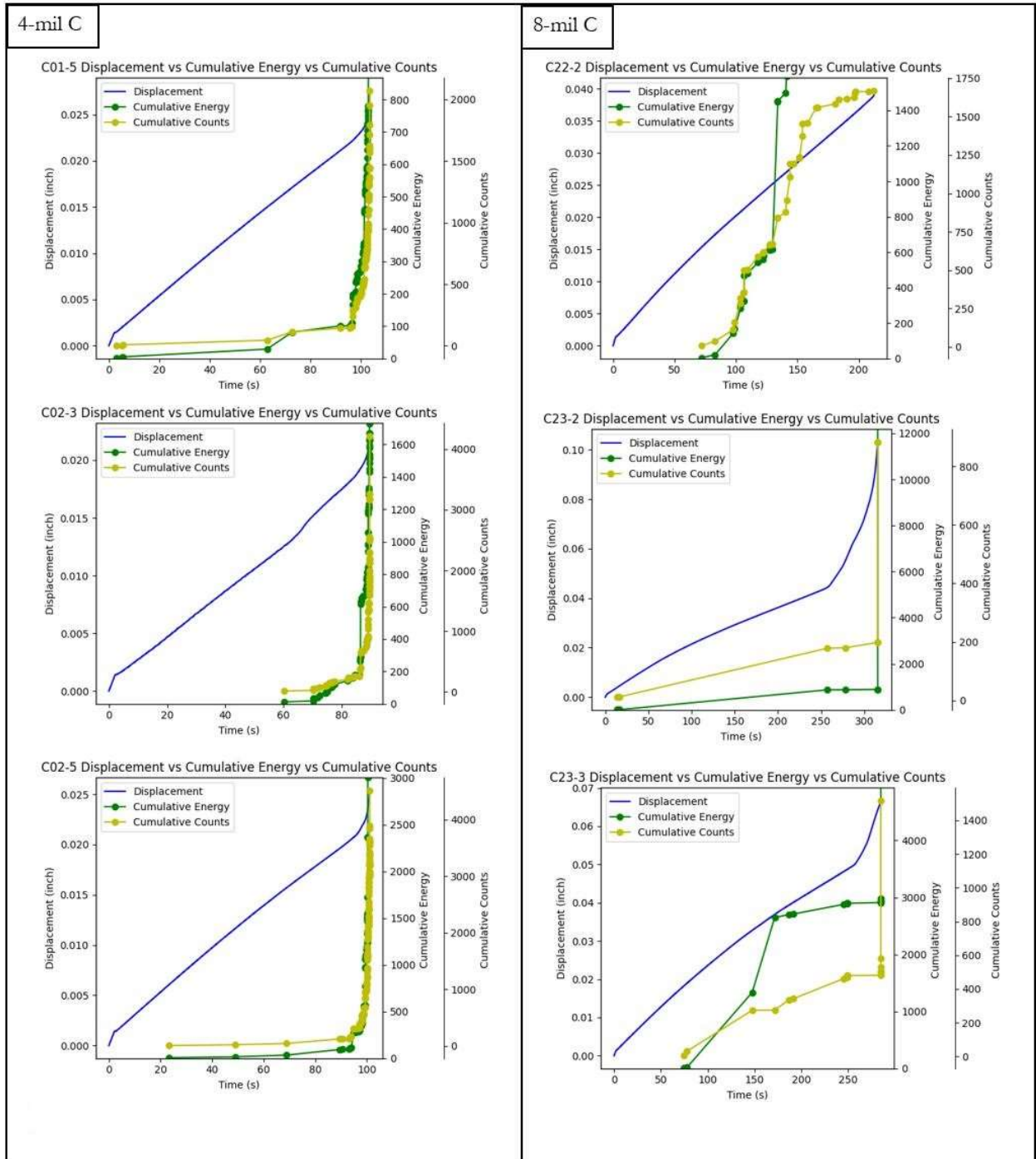
Figure 5.7: Displacement, cumulative energy, and cumulative count curves overlayed for CNT 4-mil and 8-mil
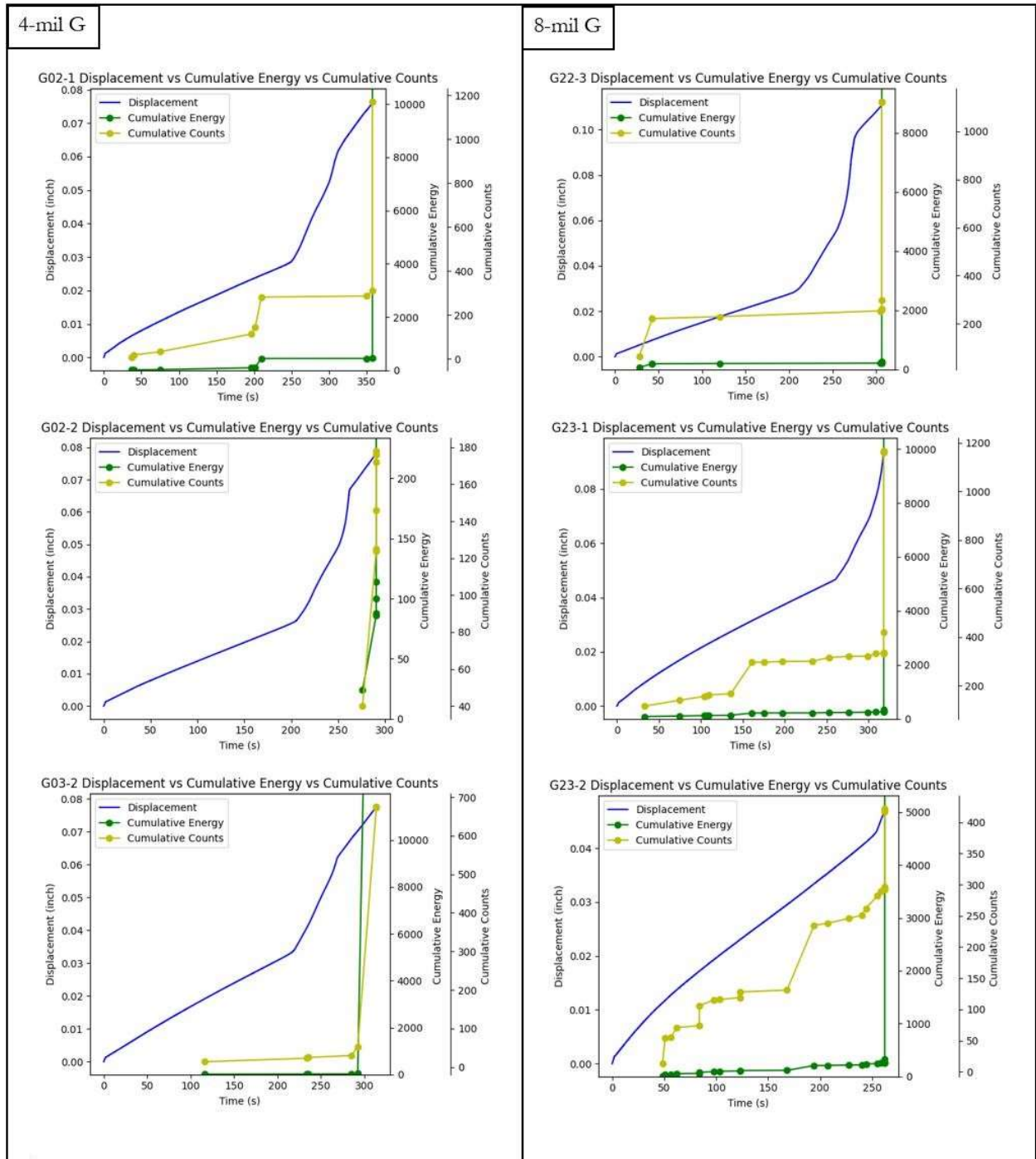
Figure 5.8: Displacement, cumulative energy, and cumulative count curves overlayed for neat GNP 4-mil and 8-mil
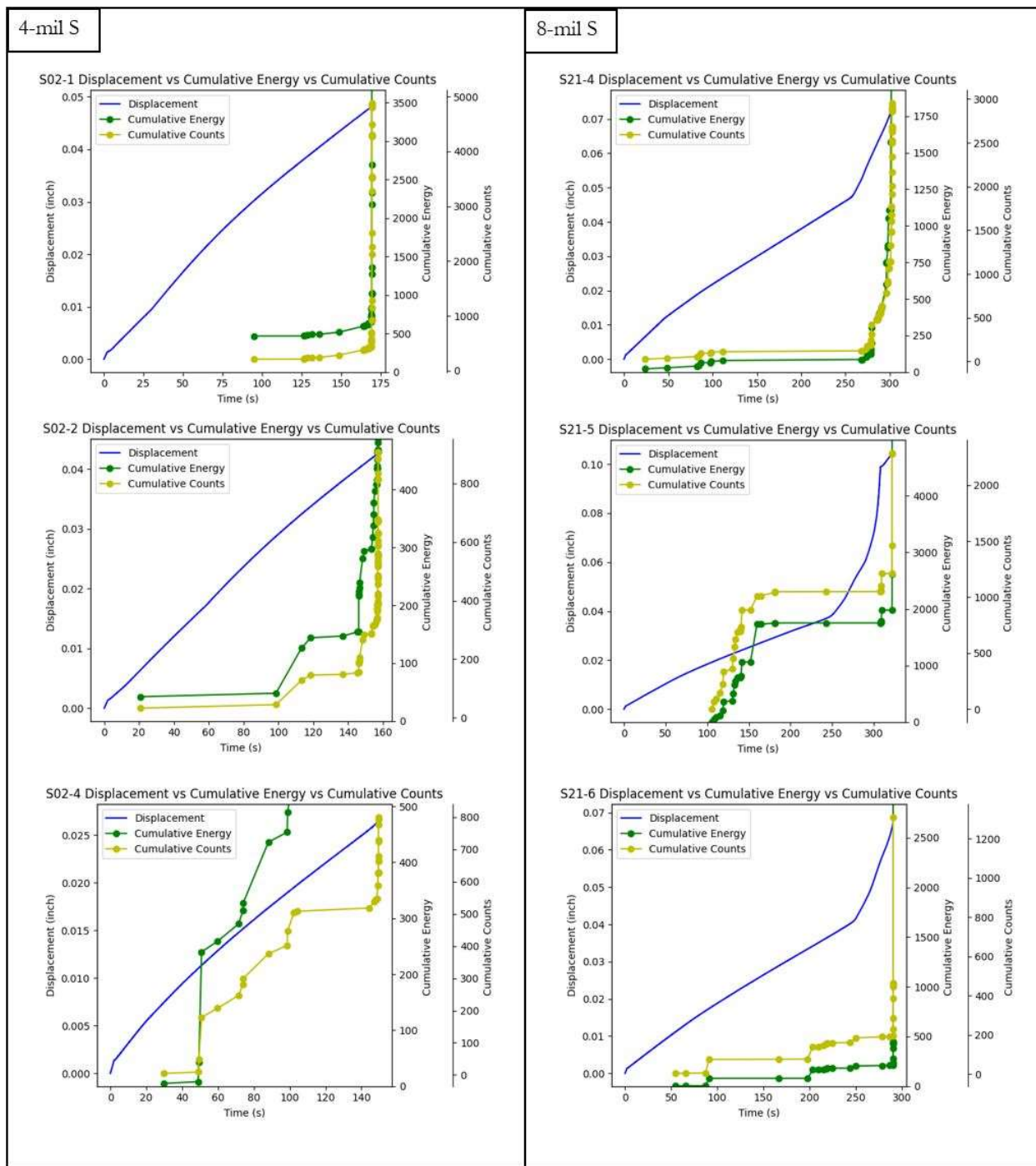
Figure 5.9: Displacement, cumulative energy, and cumulative count curves overlayed for silica 4-mil and 8-mil
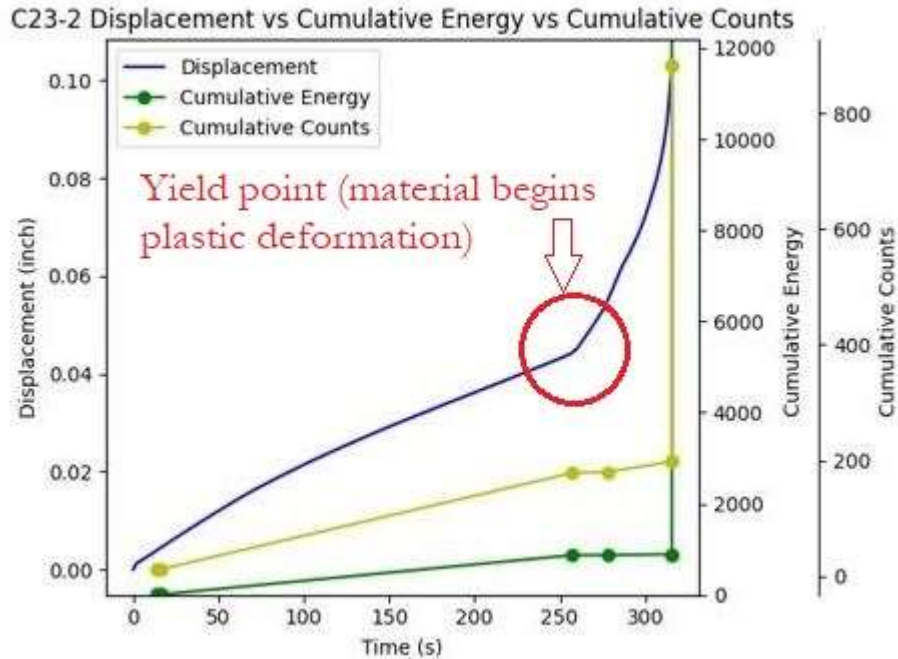
Figure 5.10: Example of yield point (accelerated, irreversible deformation) for the samples during testing.

5.3.2. Deeper Analysis of Acoustic Emission Data

To eliminate outlying data points, the last second of acoustic data collected before complete failure is omitted in the calculations for average counts risetime, signal amplitude, and total energy. This gives a more accurate story of what the materials experienced rather than the large final signals during pull-off. Table 5.3 shows the computed data. The data labels include "modified" to designate the omittance of the final second of data. Energy ratio refers to the percentage of acoustic energy generated prior to the last second of sample failure. The equation (5.2) is as follows:

Energy Ratio (%) = Σ(AE energy collected at time t-1)/ Σ(AE energy collected at time t)   (5.2)

Where t=time of sample failure (s)

Table 5.3: Modified Acoustic Emission Data

Sample	Modified Counts	Modified Risetime	Modified Amplitude	Modified Energy	Energy Ratio
E02-3	845	124	54.5	798	87.31%
E03-3	869	234	55.6	1525	2.15%
E05-3	1874	155	57.6	726	2.01%
Avg.	**1196**	**171**	**55.9**	**1016**	**30.49%**
E21-5	1662	146	52.7	117	0.38%
E22-5	177	243	58.6	2855	5.47%
E24-3	480	102	59.0	169	0.38%
Avg.	**773**	**164**	**56.8**	**1047**	**2.07%**
C01-5	547	216	50.5	667	6.58%
C02-3	699	329	51.5	813	1.60%
C02-5	547	292	52.0	3006	8.90%
Avg.	**598**	**279**	**51.3**	**1495**	**5.69%**
C22-2	92	210	56.3	3047	99.58%
C23-2	857	186	66.0	870	1.85%
C23-3	118	95	56.7	2898	7.05%
Avg.	**356**	**164**	**59.7**	**2272**	**36.16%**
G02-1	286	150	57.9	444	0.85%
G02-2	40	55	58.0	24	3.35%
G03-2	50	172	51.0	40	0.09%
Avg.	**125**	**126**	**55.6**	**169**	**1.43%**
G22-3	253	574	55.0	211	0.45%
G23-1	330	154	51.8	256	0.45%
G23-2	183	118	50.9	178	0.55%
Avg.	**255**	**282**	**52.6**	**215**	**0.48%**
S02-1	424	187	53.2	631	4.17%
S02-2	329	342	49.6	410	46.02%
S02-4	545	180	54.6	591	77.97%
Avg.	**433**	**236**	**52.5**	**544**	**42.72%**
S21-4	1324	170	55.5	1571	28.48%
S21-5	1200	165	62.1	1977	3.29%
S21-6	183	358	52.0	208	0.32%
Avg.	**902**	**231**	**56.5**	**1252**	**10.69%**

Furthermore, Table 5.4 displays the percent increase or decrease in the samples compared across the 2 thicknesses. It is shown that:

1. Average modified energy increases as thickness increases across all samples.

2. Adhesion failure area decreased as thickness increased among all reinforced samples

3. Cohesion failure area increased as thickness increased among all reinforced samples

Table 5.4: Percent Increase or Decrease by Variable Relative to Increased Sample Thickness

Sample Set	Modified Energy	Adhesion Failure Area	Cohesion Failure Area	Glue Failure Area
E	3.02%	8.89%	-19.64%	-3.25%
C	51.92%	-27.84%	237.80%	43.92%
G	26.97%	-12.47%	47.82%	-28.22%
S	130.15%	-36.75%	22.65%	191.71%

5.3.3. Summary of Acoustic Emission Used as Adhesion Failure Characterization

The volume of data collected by AE gives insight into what a material experiences during mechanical failure. The observations made on the collected data displays relationships between the sample sets as their thickness is increased and relationships across all the data. Using the AE data in conjunction with the loading and imaging data, further conclusions are drawn in the following chapter.

CHAPTER 6. SUMMARY, CONCLUSIONS, AND PROPOSED FUTURE DIRECTIONS

6.1. Summary

The mechanisms that influence a coating's adhesion to its substrate is not fully understood. Not visible to the human eye under most circumstances, the coating-substrate interface is a difficult area to characterize during mechanical failure. In this study, acoustic emission technology and imaging software was used to quantify mechanical adhesion failure between epoxy nanocomposite coating systems and mild steel. The method used to mechanically fail the coatings was a modified version of the ASTM D4541 standard. To investigate this phenomenon more effectively, thermoset epoxy resin was crosslinked and modified with three different nanoparticle reinforcements to be used as the test specimens. Adhesion performance between the coating systems was quantified using loading data, imaging, and acoustic emission data to form comprehensive conclusions. Neat epoxy was used as a control specimen in the testing.

6.2. Conclusions

Neat epoxy (EPON 828) and epoxy modified with 1% wt. carbon nanotubes, graphene nanoplatelets, and nano silicon dioxide, all at thicknesses of both 4-mil and 8-mil were the coating systems tested in this experiment. Mechanical adhesion failure was measured by loading data received from a tensile testing machine, imaging data obtained from ImageJ software, and acoustic emission data received from sensors placed on the specimens. The following conclusions can be drawn from this study.

1. The inclusion of nanoparticles into the epoxy coating matrix inevitably increases its effective adhesion strength at high enough thicknesses.

2. Agglomerates play a major role in coating-substrate adhesion. Two-dimensional nanoparticle agglomerates present less of a reduction in adhesion strength than one- or three-dimensional reinforcement.

3. Cohesion failure surface area increased among all reinforced samples as thickness increased.

4. Total average acoustic energy experienced in the specimens increased as thickness went from 4-mils to 8-mils by 3%, 52%, 27%, and 130% for neat epoxy, CNT, GNP, and silica, respectively. Therefore, it can be reasonably stated that and increase in cohesive failure area corresponds to an increase in generated acoustic energy during mechanical adhesion failure. Although more testing needs to be conducted to further verify the results, non-destructive mechanical adhesion characterization of nanocomposite coatings can give new insight and tools to coating engineers and scientists as they continue to fabricate and characterize new products for mechanical and corrosion protection.

6.3. Possible Research Directions

To further enhance this research, proposed research modifications are presented:

1. Additional modifications to the pull-off methods to make it more standardized.

2. Utilizing different sensors for the acoustic emission technology such as wideband sensors to catch a wider range of AE signals.

3. Imaging using a deep neural network to identify edges more effectively during the image synthesis.

4. Conduct a cathodic disbondment test with acoustic emission technology to see if it can capture delamination from water ingress or blister formation.

REFERENCES

[1]   M. V. Biezma and F. Schanack, "Collapse of steel bridges," *Journal of Performance of Constructed Facilities*, vol. 21, no. 5, pp. 398–405, 2007.

[2]   R. Buchanan, "Pipeline coatings and joint protection: a brief history, conventional thinking and new technologies," 2003.

[3]   *Economic Impact*. Accessed: Apr. 22, 2021. [Online]. Available: http://impact.nace.org/economic-impact.aspx

[4]   M. Biezma, M. Andrés, D. Agudo, and E. Briz, "Most fatal oil & gas pipeline accidents through history: A lessons learned approach," *Engineering failure analysis*, vol. 110, p. 104446, 2020.

[5]   *Highways and bridges*. Accessed: Apr. 22, 2021. [Online]. Available: https://www.nace.org/resources/industries-nace-serves/highways-bridges

[6]   D. G. Manning, "Corrosion performance of epoxy-coated reinforcing steel: North American experience," *Construction and Building Materials*, vol. 10, no. 5, pp. 349–365, 1996.

[7]   R. R. Fessler, "Pipeline corrosion," *Report, US Department of Transportation Pipeline and Hazardous Materials Safety Administration, Baker, Evanston, IL*, 2008.

[8]   S. Rana, R. Alagirusamy, and M. Joshi, "A review on carbon epoxy nanocomposites," *Journal of Reinforced Plastics and Composites*, vol. 28, no. 4, pp. 461–487, 2009.

[9]   P. Pissis, *Thermoset nanocomposites for engineering applications*. iSmithers Rapra Publishing, 2007.

[10] Z. Ahmadi, "Epoxy in nanotechnology: A short review," *Progress in Organic Coatings*, vol. 132, pp. 445–448, 2019.

[11] D. A. Anderson, "Natural Gas Transmission Pipelines: Risks and Remedies for Host Communities," *Energies*, vol. 13, no. 8, p. 1873, 2020.

[12] K. Siler-Evans, A. Hanson, C. Sunday, N. Leonard, and M. Tumminello, "Analysis of pipeline accidents in the United States from 1968 to 2009," *International Journal of Critical Infrastructure Protection*, vol. 7, no. 4, pp. 257–269, 2014, doi: https://doi.org/10.1016/j.ijcip.2014.09.002.

[13] C. Belvederesi, M. S. Thompson, and P. E. Komers, "Statistical analysis of environmental consequences of hazardous liquid pipeline accidents," *Heliyon*, vol. 4, no. 11, p. e00901, 2018, doi: https://doi.org/10.1016/j.heliyon.2018.e00901.

[14] Y. Zhu, X. Qian, Z. Liu, P. Huang, and M. Yuan, "Analysis and assessment of the Qingdao crude oil vapor explosion accident: Lessons learnt," *Journal of Loss Prevention in the Process Industries*, vol. 33, pp. 289–303, 2015, doi: https://doi.org/10.1016/j.jlp.2015.01.004.

[15] E. Vaca-Cortés, M. A. Lorenzo, J. O. Jirsa, H. G. Wheat, and R. L. Carrasquillo, "Adhesion testing of epoxy coating," *Center for transportation Research, Research Report*, no. 1265–6, pp. 1–129, 1998.

[16] N. Myshkin and A. Kovalev, "Adhesion and surface forces in polymer tribology—A review," *Friction*, vol. 6, no. 2, pp. 143–155, 2018.

[17] N. K. Myshkin and A. V. Kovalev, "Adhesion and friction of polymers," in *Polymer tribology*, World Scientific, 2009, pp. 3–37.

[18] N. K. Myshkin and M. I. Petrokovets, *Mechanical behavior of plastics: surface properties and tribology*. Marcel Dekker, New York, NY, USA, 2004.

[19] N. Myshkin, M. Petrokovets, and S. Chizhik, "Basic problems in contact characterization at nanolevel," *Tribology international*, vol. 32, no. 7, pp. 379–385, 1999.

[20] N. K. Myshkin, M. I. Petrokovets, and A. V. Kovalev, "Tribology of polymers: Adhesion, friction, wear, and mass-transfer," *Tribology International*, vol. 38, no. 11, pp. 910–921, 2005, doi: https://doi.org/10.1016/j.triboint.2005.07.016.

[21]   R.-Y. Qin and H. Schreiber, "Adhesion at partially restructured polymer surfaces," *Colloids and Surfaces A: Physicochemical and Engineering Aspects*, vol. 156, no. 1–3, pp. 85–93, 1999.

[22]   L. G. Beholz, C. L. Aronson, and A. Zand, "Adhesion modification of polyolefin surfaces with sodium hypochlorite in acidic media," *Polymer*, vol. 46, no. 13, pp. 4604–4613, 2005, doi: https://doi.org/10.1016/j.polymer.2005.03.086.

[23]   F. Awaja, M. Gilbert, G. Kelly, B. Fox, and P. J. Pigram, "Adhesion of polymers," *Progress in Polymer Science*, vol. 34, no. 9, pp. 948–968, 2009, doi: https://doi.org/10.1016/j.progpolymsci.2009.04.007.

[24]   M. N. Sathyanarayana and M. Yaseen, "Role of promoters in improving adhesions of organic coatings to a substrate," *Progress in Organic Coatings*, vol. 26, no. 2, pp. 275–313, 1995, doi: https://doi.org/10.1016/0300-9440(95)00572-2.

[25]   M. C. van der Leeden and G. Frens, "Surface properties of plastic materials in relation to their adhering performance," *Advanced engineering materials*, vol. 4, no. 5, pp. 280–289, 2002.

[26]   J. A. Kehr, "FBE pipeline and rebar corrosion coatings," 2000.

[27]   J. A. Kehr, D. G. Enos, and others, "FBE, a foundation for pipeline corrosion coatings," 2000.

[28]   B. T. Chang *et al.*, "Integrity of 3LPE pipeline coatings: Residual stresses and adhesion degradation," in *International Pipeline Conference*, 2008, vol. 48586, pp. 75–86.

[29]   E. Legghe, E. Aragon, L. Bélec, A. Margaillan, and D. Melot, "Correlation between water diffusion and adhesion loss: Study of an epoxy primer on steel," *Progress in Organic Coatings*, vol. 66, no. 3, pp. 276–280, 2009, doi: https://doi.org/10.1016/j.porgcoat.2009.08.001.

[30]   D. Mélot, G. Paugam, and M. Roche, "Disbondments of pipeline coatings and their effects on corrosion risks," *Journal of Protective Coatings & Linings*, pp. 18–31, 2009.

[31]   H. Gu *et al.*, "An overview of multifunctional epoxy nanocomposites," *Journal of Materials Chemistry C*, vol. 4, no. 25, pp. 5890–5906, 2016.

[32] H. Jeon, J. Park, and M. Shon, "Corrosion protection by epoxy coating containing multi-walled carbon nanotubes," *Journal of Industrial and Engineering Chemistry*, vol. 19, no. 3, pp. 849–853, 2013, doi: https://doi.org/10.1016/j.jiec.2012.10.030.

[33] H. S. Hedia, L. Allie, S. Ganguli, and H. Aglan, "The influence of nanoadhesives on the tensile properties and Mode-I fracture toughness of bonded joints," *Engineering Fracture Mechanics*, vol. 73, no. 13, pp. 1826–1832, 2006, doi: https://doi.org/10.1016/j.engfracmech.2006.02.013.

[34] S. Liu, L. Gu, H. Zhao, J. Chen, and H. Yu, "Corrosion resistance of graphene-reinforced waterborne epoxy coatings," *Journal of Materials Science & Technology*, vol. 32, no. 5, pp. 425–431, 2016.

[35] V. Singh, D. Joung, L. Zhai, S. Das, S. I. Khondaker, and S. Seal, "Graphene based materials: past, present and future," *Progress in materials science*, vol. 56, no. 8, pp. 1178–1271, 2011.

[36] K.-C. Chang *et al.*, "Room-temperature cured hydrophobic epoxy/graphene composites as corrosion inhibitor for cold-rolled steel," *Carbon*, vol. 66, pp. 144–153, 2014.

[37] H. Alhumade, A. Yu, A. Elkamel, L. Simon, and A. Abdala, "Enhanced protective properties and UV stability of epoxy/graphene nanocomposite coating on stainless steel," *Express Polymer Letters*, vol. 10, no. 12, p. 1034, 2016.

[38] T. Monetta, A. Acquesta, and F. Bellucci, "Graphene/epoxy coating as multifunctional material for aircraft structures," *Aerospace*, vol. 2, no. 3, pp. 423–434, 2015.

[39] X. Wang *et al.*, "Comparative study of three carbon additives: Carbon nanotubes, graphene, and fullerene-c60, for synthesizing enhanced polymer nanocomposites," *Nanomaterials*, vol. 10, no. 5, p. 838, 2020.

[40] A. Ghanbari and M. M. Attar, "A study on the anticorrosion performance of epoxy nanocomposite coatings containing epoxy-silane treated nano-silica on mild steel substrate,"

Journal of Industrial and Engineering Chemistry, vol. 23, pp. 145–153, 2015, doi: https://doi.org/10.1016/j.jiec.2014.08.008.

[41]   H. Wei *et al.*, "Adhesion and cohesion of epoxy-based industrial composite coatings," *Composites Part B: Engineering*, vol. 193, p. 108035, 2020, doi: https://doi.org/10.1016/j.compositesb.2020.108035.

[42]   S. Palraj, M. Selvaraj, K. Maruthan, and G. Rajagopal, "Corrosion and wear resistance behavior of nano-silica epoxy composite coatings," *Progress in Organic Coatings*, vol. 81, pp. 132–139, 2015, doi: https://doi.org/10.1016/j.porgcoat.2015.01.005.

[43]   S. Pourhashem, M. R. Vaezi, and A. Rashidi, "Investigating the effect of SiO2-graphene oxide hybrid as inorganic nanofiller on corrosion protection properties of epoxy coatings," *Surface and Coatings Technology*, vol. 311, pp. 282–294, 2017, doi: https://doi.org/10.1016/j.surfcoat.2017.01.013.

[44]   M. Conradi, A. Kocijan, D. Kek-Merl, M. Zorko, and I. Verpoest, "Mechanical and anticorrosion properties of nanosilica-filled epoxy-resin composite coatings," *Applied Surface Science*, vol. 292, pp. 432–437, 2014, doi: https://doi.org/10.1016/j.apsusc.2013.11.155.

[45]   W. Han, S. Chen, J. Campbell, X. Zhang, and Y. Tang, "Fracture toughness and wear properties of nanosilica/epoxy composites under marine environment," *Materials Chemistry and Physics*, vol. 177, pp. 147–155, 2016, doi: https://doi.org/10.1016/j.matchemphys.2016.04.008.

[46]   A. Nair and C. Cai, "Acoustic emission monitoring of bridges: Review and case studies," *Engineering structures*, vol. 32, no. 6, pp. 1704–1714, 2010.

[47]   F. Dahmene, S. Yaacoubi, and M. E. Mountassir, "Acoustic emission of composites structures: story, success, and challenges," *Physics Procedia*, vol. 70, pp. 599–603, 2015.

[48]   R. Liptai, D. Harris, and C. Tatro, "An introduction to acoustic emission," in *Acoustic Emission*, ASTM International, 1972.

[49] P. Chalker, S. Bull, and D. Rickerby, "A review of the methods for the evaluation of coating-substrate adhesion," *Materials Science and Engineering: A*, vol. 140, pp. 583–592, 1991.

[50] M. Conradi, A. Kocijan, M. Zorko, and I. Verpoest, "Damage resistance and anticorrosion properties of nanosilica-filled epoxy-resin composite coatings," *Progress in Organic Coatings*, vol. 80, pp. 20–26, 2015, doi: https://doi.org/10.1016/j.porgcoat.2014.11.011.

[51] D. Baltzis, O. Evaggelou, A. Lekatou, and A. Paipetis, "Acoustic Emission Feasibility Study for Carbon Epoxy Coated Aluminum Corrosion Monitoring," *Int J Metall Mater Eng*, vol. 4, no. 143, pp. 2455–2372, 2018.

[52] R. Francis, "COMPREHENDING PULL-OFF ADHESION TESTING," *Journal of Protective Coatings & Linings*, vol. 37, no. 12, pp. 22–26, 2020.

[53] M. Schilling, "Coating adhesion testing in accordance with ASTM D4541 Sticky business," *Corrosion Probe, Inc*, 2004.

[54] C. Magdaleno-López and J. de J. Pérez-Bueno, "Quantitative evaluation for the ASTM D4541-17/D7234 and ASTM D3359 adhesion norms with digital optical microscopy for surface modifications with flame and APPJ," *International Journal of Adhesion and Adhesives*, vol. 98, p. 102551, 2020, doi: https://doi.org/10.1016/j.ijadhadh.2020.102551.

[55] N. M. M. Ramos, M. L. Simões, J. M. P. Q. Delgado, and V. P. de Freitas, "Reliability of the pull-off test for in situ evaluation of adhesion strength," *Construction and Building Materials*, vol. 31, pp. 86–93, 2012, doi: https://doi.org/10.1016/j.conbuildmat.2011.12.097.

[56] M. P. Turunen, P. Marjamäki, M. Paajanen, J. Lahtinen, and J. K. Kivilahti, "Pull-off test in the assessment of adhesion at printed wiring board metallisation/epoxy interface," *Microelectronics Reliability*, vol. 44, no. 6, pp. 993–1007, 2004.

[57] S. Croll, C. Vetter, and B. Keil, "Variability of pipe coating pull-off adhesion measurements on cylindrical steel pipelines," in *Pipelines 2012: Innovations in Design, Construction, Operations, and Maintenance, Doing More with Less*, 2012, pp. 231–241.

[58] *Standard Test Method for Pull-Off Strength of Coatings Using Portable Adhesion Testers*. Accessed: May 03, 2021. [Online]. Available: https://compass.astm.org/

[59] I. Flores-Colen, J. de Brito, and F. Branco, "In situ adherence evaluation of coating materials," *Exp. Tech*, vol. 33, no. 3, pp. 51–60, 2009.

[60] A. Baldan, "Adhesion phenomena in bonded joints," *International Journal of Adhesion and Adhesives*, vol. 38, pp. 95–116, 2012, doi: https://doi.org/10.1016/j.ijadhadh.2012.04.007.

[61] G. Bahlakeh and B. Ramezanzadeh, "A detailed molecular dynamics simulation and experimental investigation on the interfacial bonding mechanism of an epoxy adhesive on carbon steel sheets decorated with a novel cerium–lanthanum nanofilm," *ACS applied materials & interfaces*, vol. 9, no. 20, pp. 17536–17551, 2017.

[62] M. Seipenbusch, S. Rothenbacher, M. Kirchhoff, H.-J. Schmid, G. Kasper, and A. Weber, "Interparticle forces in silica nanoparticle agglomerates," *Journal of nanoparticle research*, vol. 12, no. 6, pp. 2037–2044, 2010.

[63] B. Bittmann, F. Haupert, and A. K. Schlarb, "Ultrasonic dispersion of inorganic nanoparticles in epoxy resin," *Ultrasonics Sonochemistry*, vol. 16, no. 5, pp. 622–628, 2009, doi: https://doi.org/10.1016/j.ultsonch.2009.01.006.

[64] M. Uddin and C. Sun, "Improved dispersion and mechanical properties of hybrid nanocomposites," *Composites science and Technology*, vol. 70, no. 2, pp. 223–230, 2010.

[65] H. Hansmann, "Application of acoustic emission analysis on adhesion and structural problems of organic and metallic coatings," *Industrial & Engineering Chemistry Product Research and Development*, vol. 24, no. 2, pp. 252–257, 1985.

[66] M. T. I. Khan, "Structural Health Monitoring by Acoustic Emission," *Structural Health Monitoring from Sensing to Processing*, p. 23, 2018.

[67] A. G. Beattie, "Acoustic emission non-destructive testing of structures using source location techniques," *Albuquerque and Livermore*, 2013.

[68] G. Manthei, "Characterisation of acoustic emission sensors," 2010.

[69] W.-K. Wang, Y.-B. Li, Y.-N. Li, and Y. Zhang, "An Acoustic emission event determination method for acoustic emission testing of tank bottom based on cluster analysis," in *2013 IEEE/ASME International Conference on Advanced Intelligent Mechatronics*, 2013, pp. 1686–1691.

[70] *Nondestructive evaluation techniques : acoustic emission testing*. [Online]. Available: https://www.nde-ed.org/NDETechniques/AcousticEmission/AE_Theory-Wave.xhtml

[71] H. M. Tensi, "The Kaiser-effect and its scientific background," *Journal of Acoustic Emission*, vol. 22, pp. s1–s16, 2004.

[72] M. G. Sause, "Investigation of pencil-lead breaks as acoustic emission sources," 2011.

[73] V. A. D. de Almeida, F. G. Baptista, and P. R. de Aguiar, "Piezoelectric transducers assessed by the pencil lead break for impedance-based structural health monitoring," *IEEE Sensors Journal*, vol. 15, no. 2, pp. 693–702, 2014.

[74] "Standard Test Method for Pull-Off Strength of Coatings Using Portable Adhesion Testers," *ASTM Compass*. Accessed: May 06, 2021. [Online]. Available: https://compass.astm.org/